

Improving NLO-parton shower matched simulations with higher order matrix elements

Keith Hamilton

INFN, Sezione di Milano-Bicocca, Piazza della Scienza 3, 20126 Milan, Italy.

Email: keith.hamilton@mib.infn.it

Paolo Nason

INFN, Sezione di Milano-Bicocca, Piazza della Scienza 3, 20126 Milan, Italy.

Email: paolo.nason@mib.infn.it

ABSTRACT:

In recent times the algorithms for the simulation of hadronic collisions have been subject to two substantial improvements: the inclusion, within parton showering, of exact higher order tree level matrix elements (MEPS) and, separately, next-to-leading order corrections (NLOPS). In this work we examine the key criteria to be met in merging the two approaches in such a way that the accuracy of both is preserved, in the framework of the POWHEG approach to NLOPS. We then ask to what extent these requirements may be fulfilled using existing simulations, without modifications. The result of this study is a pragmatic proposal for merging MEPS and NLOPS events to yield much improved MENLOPS event samples. We apply this method to W boson and top quark pair production. In both cases results for distributions within the remit of the NLO calculations exhibit no discernible changes with respect to the pure NLOPS prediction; conversely, those sensitive to the distribution of multiple hard jets assume, exactly, the form of the corresponding MEPS results.

KEYWORDS: QCD, Monte Carlo, NLO Computations, Resummation, Collider Physics.

Contents

1. Introduction	1
2. Hardest emission cross section in POWHEG and MEPS simulations	4
3. Combining POWHEG and MEPS samples	8
3.1 Jet cross sections	8
3.2 A simple MENLOPS merging procedure	9
4. Results	11
4.1 POWHEG and MEPS simulations	12
4.2 MENLOPS implementation	13
4.3 W boson production	14
4.3.1 Jet multiplicities	14
4.3.2 Inclusive observables	17
4.3.3 Jet activity	20
4.4 Top quark pair production	25
4.4.1 Jet multiplicities	25
4.4.2 Inclusive observables	28
4.4.3 Jet activity	31
5. Conclusions	36
6. Acknowledgments	38

1. Introduction

In recent years the promise of new and exciting data from the LHC experiments has led to renewed interest and vigor in the research and development of Monte Carlo event generators. In this time significant progress has been made and a number of long standing goals have been achieved. The most significant innovations have been the inclusion of full next-to-leading order (NLO) corrections within parton shower simulations and, separately, the merging of event generators based on tree level matrix elements together with parton showers.

The central challenge to be addressed for both of these advances was that of overcounting, since the parton shower dynamics encodes the collinear limits of the relevant higher order, real and virtual, matrix elements. In the case of matching with NLO calculations a

further complication lay in how to arrange the NLO formulae such that they lend themselves to a physical, probabilistic, interpretation and hence the formulation of a practical Monte Carlo algorithm.

Currently there are two proven methods, MC@NLO and POWHEG [1–3], for including NLO corrections within parton shower algorithms. Simulations based on these approaches provide predictions for infrared safe observables with full NLO accuracy. The hardest emitted parton in each event is distributed according to the exact real, single emission, matrix elements, and NLO virtual corrections are consistently included. Moreover, effects of further, higher order, soft and collinear emissions to all orders in the leading log approximation are also included. Both methods may be considered to be mature, having been applied to several processes, and the subject of a number of comparative studies [4–15].

Despite the clear advantages associated with promoting parton shower event generators to NLO accuracy (NLOPS), this class of simulations are not, by themselves, sufficiently versatile to model all features of the data in adequate detail. In particular, since the only exact real corrections included are those of the next-to-leading order calculation, the parton shower approximation is used to describe all but one of the emissions. As such these event generators do not offer a satisfactory description of particle production in association with multiple hard jets, as is widely anticipated to occur in the case of new physics signals and backgrounds [15, 16].

The other leading advancement in this line of research greatly improves the ordinary parton shower description of a given final state in association with additional QCD radiation, by making use of higher order tree level matrix elements. These matrix element-parton shower (MEPS) merging procedures take parton level events, of assorted multiplicity, from tree level event generators and carefully dress them with parton showers, vetoing and/or weighting them in such a way as to yield inclusive event samples smoothly populating all of phase space, while not overcounting any regions. The introduction of exact high multiplicity matrix elements acts to correct the radiation pattern with respect to the standalone parton shower description. The distribution of the hard emissions, and hence the distribution of the jets, follows from the real matrix elements while only the internal structure of jets is determined by the parton shower, where previously the former was given erroneously by the multiple soft-collinear limits of those same matrix elements.

As with the NLOPS case, the MEPS methods are not without their shortcomings. Since the underlying physics ingredients from which the MEPS simulations are constructed are tree level matrix elements and leading-log resummation, they are subject to many of the same theoretical uncertainties as leading order calculations. Predictions for observables based on these calculations exhibit an acute sensitivity to the renormalization and factorization scales, predominantly affecting the overall normalization but also, to a lesser extent, the shapes of distributions. These limitations are in contrast to the NLOPS output for which the complete set of $\mathcal{O}(\alpha_S)$ corrections greatly reduces such ambiguities.

Plainly there is a high degree of complementarity between the NLOPS and MEPS schemes in regards to their strengths and weaknesses. Moreover, for both classes of event generators there now exists a significant and rapidly growing number of phenomenologically important simulations. In fact, the MEPS method has been largely automated within tree

level event generators [17–19] and further progress has been made toward automated production of NLOPS simulations [20]. It is therefore natural to look for a means of combining the two approaches, preserving their virtues and forgoing their weaknesses. This problem may be approached in several different ways. For example, if we rely upon the POWHEG method for our NLOPS approach, what we would need is a MEPS procedure that can start from a given process with a given kinematics, and builds higher multiplicity events on top of it. In other words, we would like a MEPS that behaves as any standard shower Monte Carlo program. However, current MEPS methods are not designed to work in this way. They generate full event samples with no constraints on their kinematics. So, if we want to follow this direction, we may expect that a lot of work would be needed to reformulate the whole MEPS approach.

A theoretical formalism aiming at such a merging, albeit in the same vein as the MC@NLO approach to NLOPS matching, has been proposed in Ref. [21] and an implementation realised for the process $H \rightarrow gg$ at NLO, including real emission corrections for the first radiated gluon only. A further, more ambitious endeavour, by Lavesson and Lönnblad [22], aims instead to augment the lowest order parton shower simulation with *both* higher multiplicity real *and* virtual corrections, in the spirit of [23]. For the time being, the theoretical construction and implementation is limited to the simulation of e^+e^- collisions. We shall briefly return to discuss how this last work compares to the one we shall propose at the end of Section 3.

In this paper we approach the problem of merging an MEPS simulation with an NLOPS simulation in a radically different way. We compare the MEPS and NLOPS approaches, identifying and quantifying their best features, with a view to defining what is required to obtain an exact theoretical solution of the merging problem. Motivated by the presence of the large body of validated, trusted MEPS and NLOPS simulations available today, we then seek to address the question of how close one may get to achieving a theoretically exact merging, simply by manipulating their event samples. We go on to show that in this way one may obtain a MENLOPS merging that is, in practice, very satisfactory. We will describe the application of this merging method to W boson production and to $t\bar{t}$ production in hadronic collisions.

Although the method that we propose proves to be very much adequate for practical applications, we emphasize that it is not an exact solution to the matching problem. We have however achieved two goals: firstly, we have found a practical method to merge MEPS and NLOPS simulations that can be immediately applied to processes for which such simulations already exist; second, we have clarified what is needed in order to achieve a full theoretical solution of the merging problem.

We begin in Section 2 by briefly reviewing key features of the POWHEG formalism, in particular the hardest emission cross section. We do not provide a summary of the methods used to implement MEPS algorithms. We will simply assume that we have at hand an MEPS simulation that is capable of predicting small angle radiation with the same accuracy as a shower Monte Carlo program and, at the same time, also has the ability to describe high multiplicity jet production with leading order accuracy. Based upon these assumptions, we derive a cross section differential in the phase space variables associated

with the hardest emitted parton in the MEPS approach. On this basis, we formulate an exact theoretical solution to the matching problem. In Section 3 we formulate our practical matching prescription and, based upon the findings in Section 2, we derive its range of applicability. In Section 4 we demonstrate the efficacy of our approach using W boson and top-quark pair production as case studies, elaborating on the conditions necessary for its success. Our findings and conclusions are summarized in Section 5.

2. Hardest emission cross section in POWHEG and MEPS simulations

Since we shall frequently use the term *NLO accuracy* in the course of this work, and since the way in which this is manifest in NLOPS simulations generalises that of, more familiar, fixed order calculations, before we begin, we wish to take a moment to clarify what we mean by it. As an instructive example consider the case of W production in hadronic collisions. At leading order in perturbation theory, the cross section is of zeroth order in the strong coupling constant and the transverse momentum of the W is zero. When $\mathcal{O}(\alpha_S)$ corrections to the LO process are included, inclusive observables that do not vanish at the Born level are predicted with NLO accuracy, while those that do vanish are only known with LO accuracy. Thus, for example, the prediction for the W production cross section with the constraint $p_T^W < p_T^{\text{cut}}$ is comprised of contributions of order 1 and order α_S , it is thus known with NLO accuracy. On the other hand, the cross section with the cut $p_T^W > p_T^{\text{cut}}$ vanishes at the Born level, thus the NLO calculation of W production only yields a leading order accurate prediction for this observable. Here, our use of the term NLO accuracy is restricted to inclusive observables that do not vanish at the Born level.

We further remark that, in NLOPS simulations, in contrast to fixed order calculations, the distinction made above is slightly more subtle. While in the fixed order NLO calculation the virtual contribution to the cross section in our example sits at the point $p_T = 0$, in an NLOPS simulation it is spread out over the whole Sudakov region of the p_T distribution. NLO accuracy is thus also spread out in this region in a physically consistent way.

The basic ideas behind the POWHEG method are most readily introduced in the context of a simple example wherein the leading order process is comprised of a single colour dipole with a massless parton. One can consider, for definiteness, the top quark decay process $t \rightarrow bW$, neglecting the b quark mass and taking the W boson to be stable. In general we denote the leading order differential cross section $B(\Phi_B)$, corresponding, in our example, to that of the $t \rightarrow bW$ process, parametrized by the so-called Born phase space variables Φ_B . The differential cross section for the real emission process is similarly denoted $R(\Phi_R)$, where the phase space variables, Φ_R , determine the kinematics of the relevant processes; they are routinely defined in terms of the Born phase space variables Φ_B together with additional radiative phase variables Φ_{rad} *i.e.* $\Phi_R = \Phi_R(\Phi_B, \Phi_{\text{rad}})$. In the context of our heuristic example, the Born phase space is characterized by the direction of the W, while the radiation phase space may be described by the angle of the emitted gluon with respect to the W direction, its azimuth and its energy.

In the POWHEG approach [2], the simulation process starts with the generation of a

two or three body final state according to the distribution

$$d\sigma_{\text{PW}}^{\text{HE}} = \overline{B}(\Phi_B) d\Phi_B \left[\Delta_R(p_T^{\text{min}}) + \frac{R(\Phi_R)}{B(\Phi_B)} \Delta_R(k_T(\Phi_R)) d\Phi_{\text{rad}} \right], \quad (2.1)$$

that represents the cross section for the hardest radiated particle in the inclusive process.¹ The function $\overline{B}(\Phi_B)$ is defined as

$$\overline{B}(\Phi_B) = B(\Phi_B) + \left[V(\Phi_B) + \int d\Phi_{\text{rad}} R(\Phi_R) \right], \quad (2.2)$$

where $B(\Phi_B)$ is the leading order contribution. The virtual term $V(\Phi_B)$ has soft and collinear divergences that cancel against the integral of the real term over the radiation variables. We thus assume that, within the square bracket, some regularization procedure (like dimensional regularization) is adopted. The technicalities concerning how this formula is realised in POWHEG are highly complex; however, they are not directly relevant to the present discussion (such details can be found in *e.g.* Refs. [3, 20]). The modified Sudakov form factor is defined as

$$\Delta_R(p_T) = \exp \left[- \int d\Phi_{\text{rad}} \frac{R(\Phi_R)}{B(\Phi_B)} \theta(k_T(\Phi_R) - p_T) \right], \quad (2.3)$$

where $k_T(\Phi_R)$ is equal to the transverse momentum of the extra parton in the collinear and soft limits. We implicitly assume, as in a conventional parton shower simulation, that k_T has always an implicit lower cut-off p_T^{min} in Eq. 2.1. Note also that the explicit dependence of Δ_R on Φ_B has been suppressed for ease of notation.

We now briefly recount the key features of the POWHEG formula through which NLO accuracy is achieved. First of all, in the large transverse momentum region, the hardest emission cross section Eq. 2.1 becomes, up to terms of higher order, equal to $R(\Phi_R)$. In fact, for large transverse momenta only the second term in the square bracket of Eq. 2.1 contributes. Furthermore, the associated Sudakov form factor tends to one. Hence, for these kinematics, neglecting terms beyond NLO accuracy, we have

$$d\sigma_{\text{PW}}^{\text{HE}} = \overline{B}(\Phi_B) \frac{R(\Phi_R)}{B(\Phi_B)} d\Phi_B d\Phi_{\text{rad}} \approx R(\Phi_R) d\Phi_R. \quad (2.4)$$

Of equal importance in achieving NLO accuracy is the requirement that the integral of the POWHEG hardest emission cross section with respect to the radiative phase space variables should be identical to that of the exact NLO cross section, *i.e.* equal to Eq. 2.2. This property is guaranteed by the form of the POWHEG Sudakov form factor which, by construction, satisfies the following identity

$$\frac{d\Delta_R(p_T)}{dp_T} = \Delta_R(p_T) \int \frac{R(\Phi_R)}{B(\Phi_B)} \delta(k_T(\Phi_R) - p_T) d\Phi_{\text{rad}}. \quad (2.5)$$

Using this relation it is trivial to show that the term in square brackets in Eq. 2.1 integrates to one for all Φ_B .

¹The superscript HE stands here for “hardest emission”.

Note that taking the Sudakov form factor exactly as laid out in the original POWHEG proposal [2] is not a strict requirement for attaining NLO accuracy, merely the most convenient one. A modified POWHEG formula

$$d\sigma_{\text{PW}}^{\text{HE}} = \overline{B}(\Phi_B) d\Phi_B \left[\frac{\Delta_S(p_T^{\min}) + d\Phi_{\text{rad}} \frac{R(\Phi_R)}{B(\Phi_B)} \Delta_S(k_T(\Phi_R))}{\Delta_S(p_T^{\min}) + \int d\Phi_{\text{rad}} \frac{R(\Phi_R)}{B(\Phi_B)} \Delta_S(k_T(\Phi_R))} \right], \quad (2.6)$$

where $\Delta_S(p_T)$ is an alternative Sudakov form factor given by

$$\Delta_S(p_T) = \exp \left[- \int d\Phi_{\text{rad}} \frac{S(\Phi_R)}{B(\Phi_B)} \theta(k_T(\Phi_R) - p_T) \right], \quad (2.7)$$

would satisfy the same properties as Eq. 2.1, provided that $S(\Phi_R)$ coincides with $R(\Phi_R)$ in the regions of phase space corresponding to soft and collinear emissions. In other words, to achieve NLO accuracy it is mandatory that the term in square bracket is unitary, *locally* in the Born phase space. However, there is some flexibility regarding precisely how that unitarity is achieved.

In the POWHEG framework the parton shower simulation is promoted to NLO accuracy by distributing non-radiative events according to the first term in Eq. 2.1 and the hardest (highest p_T) emission according to the second term. Whereas in a conventional parton shower simulation, an N -body configuration is generated according to $B(\Phi_B)$ and then showered using a conventional, process-independent, Sudakov form factor, the POWHEG technique requires that the N -body configuration is generated instead according to $\overline{B}(\Phi_B)$ and showered with the process-dependent modified Sudakov form factor in Eq. 2.3. Inclusive observables computed using events generated from this distribution have full NLO accuracy, in contrast to the corresponding predictions from a conventional parton shower simulation, which are only LO accurate.

With these points in mind we move to express, in similar terms, the analogous cross section in MEPS based simulations. In this way we aim to clarify the differences between the MEPS and POWHEG methods, in order to guide us in attempting to consistently combine the two. To this end, we need only assume that event generators which utilise these merging methods, are capable of correctly describing widely separated jets of any multiplicity according to the leading order matrix elements, and small angle radiation according to the leading logarithmic approximation. In simpler words, we will assume that MEPS algorithms have the same accuracy as a shower Monte Carlo in the small angle limit, and leading order QCD accuracy for jet cross sections, even for widely separated jets.

Momentarily, putting aside the fact that a very small fraction of events contain no radiation at all, given an otherwise arbitrary MEPS event, we may cluster it according to a k_\perp jet algorithm, until it is resolved as a 1-jet event. The kinematics of this 1-jet structure may be parametrized in terms of the real emission phase space Φ_R , which may in turn be expressed in terms of the Born and radiative phase space variables Φ_B and Φ_{rad} introduced earlier. Effectively the jet algorithm defines a pair of *unique* mappings $\hat{\Phi}_B(\Phi)$ and $\hat{\Phi}_{\text{rad}}(\Phi)$ from the phase space of arbitrary multiplicity MEPS events, generically denoted Φ , to the Born and radiative phase spaces respectively.

Having specified the Born and radiative phase space projections, the MEPS hardest emission cross section, for radiative events, follows as

$$\begin{aligned} & \int d\Phi \frac{d\sigma_{\text{ME}}}{d\Phi} \delta\left(\Phi_B - \widehat{\Phi}_B(\Phi)\right) \delta\left(\Phi_{\text{rad}} - \widehat{\Phi}_{\text{rad}}(\Phi)\right) \\ &= \widehat{R}(\Phi_R) \Delta_{\widehat{R}}(k_T(\Phi_R)), \end{aligned} \quad (2.8)$$

where $\widehat{R}(\Phi_R)$ differs from $R(\Phi_R)$ by a factor $1 + \mathcal{O}(\alpha_S)$. $\Delta_{\widehat{R}}(k_T(\Phi_R))$ is an effective Sudakov form factor, of equivalent logarithmic accuracy to those used in POWHEG and conventional parton shower simulations. Equation (2.8) follows directly from our assertions regarding the MEPS algorithms, namely, that widely separated jets are described with leading order accuracy (this is why we recover $R(\Phi_R)$ up to terms formally of higher order in α_S), while radiation in the soft and collinear regions must be described as accurately as in a parton shower Monte Carlo (this is why we recover the $\Delta_{\widehat{R}}(k_T(\Phi_R))$ factor). The difference between the real emission cross section used in NLO calculations, $R(\Phi_R)$, and the MEPS approximation to it, $\widehat{R}(\Phi_R)$, arises from spurious higher order terms, of NNLO significance, that will in general be present in an MEPS algorithm.

We can now express the hardest jet cross section in an MEPS simulation in a similar form to that of the POWHEG hardest emission cross section *viz*

$$d\sigma_{\text{ME}}^{\text{HE}} = B(\Phi_B) d\Phi_B \left[\Delta_{\widehat{R}}(p_T^{\min}) + \frac{\widehat{R}(\Phi_R)}{B(\Phi_B)} \Delta_{\widehat{R}}(k_T(\Phi_R)) d\Phi_{\text{rad}} \right]. \quad (2.9)$$

Following the manipulations leading to Eq. 2.6 we proceed to rewrite the MEPS cross section in such a way that the piece corresponding to the generation of the radiation is manifestly unitary:

$$d\sigma_{\text{ME}}^{\text{HE}} = \overline{B}_{\text{ME}}(\Phi_B) d\Phi_B \frac{\Delta_{\widehat{R}}(p_T^{\min}) + \int d\Phi_{\text{rad}} \frac{\widehat{R}(\Phi_R)}{B(\Phi_B)} \Delta_{\widehat{R}}(k_T(\Phi_R))}{\Delta_{\widehat{R}}(p_T^{\min}) + \int d\Phi_{\text{rad}} \frac{\widehat{R}(\Phi_R)}{B(\Phi_B)} \Delta_{\widehat{R}}(k_T(\Phi_R))}, \quad (2.10)$$

where

$$\overline{B}_{\text{ME}}(\Phi_B) = B(\Phi_B) \left[\Delta_{\widehat{R}}(p_T^{\min}) + \int d\Phi_{\text{rad}} \frac{\widehat{R}(\Phi_R)}{B(\Phi_B)} \Delta_{\widehat{R}}(k_T(\Phi_R)) \right]. \quad (2.11)$$

It is also clear that

$$\overline{B}_{\text{ME}}(\Phi_B) = \Delta_{\widehat{R}}(p_T^{\min}) + \int d\Phi \frac{d\sigma_{\text{ME}}}{d\Phi} \delta\left(\Phi_B - \widehat{\Phi}_B(\Phi)\right). \quad (2.12)$$

We thus state the following simple result: in order to achieve NLO accuracy in a MEPS simulation it is sufficient to reweight the events with a factor

$$\frac{\overline{B}(\widehat{\Phi}_B(\Phi))}{\overline{B}_{\text{ME}}(\widehat{\Phi}_B(\Phi))}, \quad (2.13)$$

where, as before, Φ represents the kinematics of an arbitrary multiplicity MEPS event and \overline{B}_{ME} is given by Eq. 2.12.

Although easy to state, Eq. 2.13 may turn out in practice to be very difficult to use. In fact, only for simple processes one may be able to compute the ratio $\bar{B}/\bar{B}^{\text{ME}}$ and store it in a sufficiently dense grid of points in the Born phase space, such that given any Born phase space configuration the value of the ratio may be interpolated with enough precision.

3. Combining POWHEG and MEPS samples

In this section we shall first discuss the relative merits of jet cross sections and their constituent events in NLOPS and MEPS simulations. Based on the exact merging outlined in Section 2 and the following jet cross section analysis, we propose an approximate MENLOPS scheme requiring no modifications to existing codes. As we shall see later, for some LHC processes the exact approach we advocated earlier can be totally obviated by this simplified scheme.

3.1 Jet cross sections

We will now examine the POWHEG and MEPS samples by clustering their events according to a given jet resolution scale y_0 . We assume that the clustering parameter is related to the transverse momentum *i.e.* that it is of the Durham variety. The events will be thus characterized by the number of jets at the given y_0 value. We will still stick to our example, where only a single massless coloured parton is present in the external leg of our basic process. We begin by comparing the differential cross sections for the production of events in which no additional radiated jets are present. In POWHEG, this is given by

$$d\sigma_{\text{PW}}(0) = \bar{B}(\Phi_B) d\Phi_B \left[\Delta_R(p_T^{\min}) + \int d\Phi_{\text{rad}} \frac{R(\Phi_R)}{B(\Phi_B)} \Delta_R(k_T(\Phi_R)) \theta(y_0 - y(\Phi_R)) \right], \quad (3.1)$$

depending upon the Born variables alone. Equation 3.1 is obtained by assuming that clustering showered POWHEG events to the point where only one radiated jet is resolved recovers the basic POWHEG cross section Eq. 2.1. This is certainly the case for the non-emission term, and also for the radiation term, since when POWHEG is interfaced to a parton shower Monte Carlo it is forbidden to generate radiation harder than the POWHEG generated one. Formula 3.1 is clearly leading-log accurate when y_0 is very small. Appealing to unitarity it can be rewritten in the following way

$$d\sigma_{\text{PW}}(0) = \bar{B}(\Phi_B) d\Phi_B \left[1 - \int d\Phi_{\text{rad}} \frac{R(\Phi_R)}{B(\Phi_B)} \Delta_R(k_T(\Phi_R)) \theta(y(\Phi_R) - y_0) \right]. \quad (3.2)$$

When y_0 is not small, the factor in square bracket differs from one by terms of order α_s , and the full formula is accurate at NLO.

The corresponding cross section in the MEPS simulation is given by an expression of the form

$$d\sigma_{\text{ME}}(0) = \bar{B}_{\text{ME}}(\Phi_B) d\Phi_B \left[1 - \int d\Phi_{\text{rad}} \frac{\hat{R}(\Phi_R)}{\bar{B}_{\text{ME}}(\Phi_B)} \Delta_{\hat{R}}(k_T(\Phi_R)) \theta(y(\Phi_R) - y_0) \right], \quad (3.3)$$

where $\Delta_{\hat{R}}$ is an effective Sudakov form factor accounting for the combination of the ME and PS Sudakov form factors in the MEPS algorithm and, for brevity, $\Phi_B = \hat{\Phi}_B(\Phi)$. Thus, from the point of view of NLO accuracy, the MEPS result differs from the POWHEG one by the weight factor in Eq. 2.13, with remaining differences, due to the terms in the square brackets, being of relative order α_s^2 . Moreover, we point out that this weight factor is in fact the *only* difference between the MEPS result and that which would be obtained using the exact merging procedure outlined in Section 2. It is therefore clear that the POWHEG prediction for this quantity is always better than the MEPS one.

We now examine the cross section for radiating a single additional jet. In POWHEG it is given by

$$d\sigma_{\text{PW}}(1) = \overline{B}(\Phi_B) d\Phi_B \left[\frac{R(\Phi)}{B(\Phi_B)} \Delta_R(k_T(\Phi)) \theta(y(\Phi) - y_0) d\Phi_{\text{rad}} \right] \Delta_{\text{MC}}(y_0). \quad (3.4)$$

This is equivalent to the cross section for the first radiation to be above the clustering scale, times and extra factor $\Delta_{\text{MC}}(y_0)$, that represents the probability that the subsequent shower does not generate more jets. It is often stated that, as far as the radiation cross section is concerned, MEPS and POWHEG are equivalent. This is certainly the case if the clustering scale y_0 is large enough. In this limit $\Delta_{\text{MC}}(y_0)$ differs from 1 by terms of higher order, and the one jet cross section itself becomes of order α_s . However, as the clustering scale becomes smaller, and the fraction of one jet events becomes a sizeable fraction of the total cross section, we should recall that an NLO K -factor becomes visible in the POWHEG cross section that is not present in the MEPS one. Thus, there is at least one limiting case in which the POWHEG cross section is better than the MEPS one, and so POWHEG should be preferred for this quantity.

As we go to higher jet multiplicity, however, the MEPS becomes more accurate than the POWHEG approach. In fact, the cross section for more than one jet is determined in the POWHEG approach in part by the generation of the hardest jet, and in part by the shower Monte Carlo, that will generate the second jet. The whole cross section will thus be accurate only in the kinematic region where the second jet is either collinear to the first jet, or (depending upon the Shower Monte Carlo ability to predict correctly soft emissions) when it is soft. On the other hand, in the MEPS approach, this cross section will be correctly predicted at all angles.

3.2 A simple MENLOPS merging procedure

Based on our deductions in Section. 3.1, regarding the accuracy of the jet cross sections and the description of the events which comprise them, we propose that the exact reweighting method outlined in Section 2 may be very well approximated by simply mixing the 0- and 1-jet events output from a POWHEG simulation, together with events including at least two jets output from an MEPS simulation. If the fraction of events with more than one jet in the final MENLOPS sample is at least as small as α_s relative to the total, NLO accuracy for shape variables will be clearly preserved, and the LO description of high multiplicity jet samples will also be retained.

The proportions in which the various contributions should be mixed are non-trivial, they are chosen so as to respect our assertions regarding the accuracy of the various jet cross sections in the different approaches. Let us denote the total POWHEG cross section for j jets by $\sigma_{\text{PW}}(j)$ and the corresponding MEPS cross section by $\sigma_{\text{ME}}(j)$. By analogy we label the fully differential cross section for POWHEG events containing j jets by $d\sigma_{\text{PW}}(j)$, and that of their MEPS counterparts by $d\sigma_{\text{ME}}(j)$. Note that, by fully differential, we mean differential in the momenta of *all* produced particles, after showering has taken place. In other words,

$$d\sigma_{\text{PW}} = \sum_j d\sigma_{\text{PW}}(j) \quad (3.5)$$

represents the differential cross section for multi-particle production as simulated by the POWHEG algorithm. We also use the notation $(\geq j)$ to indicate the total or differential cross section for a number of jets greater than or equal to j . We build a sample by combining MEPS and POWHEG event samples according to their jet multiplicities in the following proportions

$$d\sigma = d\sigma_{\text{PW}}(0) + \frac{\sigma_{\text{ME}}(1)}{\sigma_{\text{ME}}(\geq 1)} \frac{\sigma_{\text{PW}}(\geq 1)}{\sigma_{\text{PW}}(1)} d\sigma_{\text{PW}}(1) + \frac{\sigma_{\text{PW}}(\geq 1)}{\sigma_{\text{ME}}(\geq 1)} d\sigma_{\text{ME}}(\geq 2). \quad (3.6)$$

Notice that the total cross section for the combined sample equals that of POWHEG. Plainly the 0-jet cross section is as generated by POWHEG alone, as is the 1-jet cross section, except for the overall factor

$$\frac{\sigma_{\text{ME}}(1)}{\sigma_{\text{ME}}(\geq 1)} \frac{\sigma_{\text{PW}}(\geq 1)}{\sigma_{\text{PW}}(1)}. \quad (3.7)$$

In other words, the total 1-jet fraction is corrected, as if it was assumed that the ratio of the 1-jet fraction to the ≥ 1 -jet fraction is better determined by the MEPS program. This is in fact the case if y_0 is not too small. The cross section for two or more jets is instead given by

$$d\sigma(\geq 2) = \frac{\sigma_{\text{PW}}(\geq 1)}{\sigma_{\text{ME}}(\geq 1)} d\sigma_{\text{ME}}(\geq 2), \quad (3.8)$$

i.e. it carries an extra overall K -factor with respect to the bare MEPS result, given precisely by the NLO K -factor for the ≥ 1 -jet cross section.

We now discuss to what extent the procedure outlined above retains the best features of the POWHEG and MEPS approaches. There are two questions to answer. The first one is to what extent the proposed procedure yields the correct NLO cross sections for inclusive quantities. The second one is to what extent jet cross sections for widely separated jets are generated according to the exact leading order matrix elements. As far as NLO accuracy is concerned, it is clear that a problem may arise from the (≥ 2) sample. The contribution of this sample to inclusive quantities does not include the NLO corrections with their full dependence on the underlying Born kinematics. It thus violates the NLO accuracy of the calculation. However, if y_0 is not too small, the ≥ 2 jets contribution to the cross section is, relatively, an effect of order α_s^2 . It is enough for us to choose y_0 such that this fraction is not larger than α_s to maintain NLO accuracy of the full sample. Observe also that the presence of the K factor in Eq. 3.8 improves the situation. In other words, even if we

are not capable to correct the ≥ 2 jets sample with the factor of Eq. 2.13, we can at least correct the overall rate in such a way that if the factor in Eq. 2.13 is constant the correction becomes exact. Conversely, the ≥ 2 -jet sample is certainly accurate for jet production at large angles and with large multiplicity. The 0- and 1-jet samples, however, can have jet substructures at relatively large angles, that thus violate ME accuracy. This is certainly the case if y_0 is too large. In practice, we must thus require y_0 to have a value which is small enough to be acceptable for MEPS matching, but large enough so that the ≥ 2 jet sample comprises a relative fraction no greater than $\mathcal{O}(\alpha_s)$. Notice that also in this case we apply a constant correction factor to the 1-jet fraction, such that the ratio of 1 to ≥ 1 jet is equal to the MEPS prediction.

The tension in the choice of y_0 (neither too large, nor too small) is what prevents this method from being an exact solution to the MEPS-NLOPS merging problem. As in typical MEPS matching methods, one expects that making the clustering parameter small should yield at some point the correct answer. This is not the case in the present method. By making y_0 too small the fraction of ≥ 2 jet events becomes substantial, yielding a contribution that does not correctly include the NLO corrections (in order for it to be correct at NLO, we would need to include the factor in Eq. 2.13, whereas we only include a constant K -factor).

We now briefly comment on the method of Ref. [22], which differs markedly from our approach. NLO accuracy is achieved there by computing jet distributions at NLO to begin with, using a clustering scale called y_{MS} . In order for the method to work, this clustering scale has to be set large enough so that most of the Sudakov region is already included by it; in the example of W production, this means that the 0-jet cross section should already include most of the total cross section. This is more restrictive than in our method, for which we only require that most of the total cross section be confined to the 0- and 1-jet samples, thereby allowing for a lower merging scale.

In finishing, we wish to emphasize that, as far as the most simple processes are concerned, a complete solution of the merging problem straightforwardly follows from the discussion presented so far. For example, in case of Higgs production, the underlying Born kinematics depends upon a single parameter. In the FKS implementation of POWHEG for Higgs production, such parameter is the rapidity of the Higgs. One can easily compute and parametrize the factor in Eq. 2.13, and use it to reweight the ME sample. For more complex processes, we have at least clarified what corrections are needed to obtain a full solution to the matching problem. However, from the studies reported in the following pages, we also stress that, depending on the process, the practical gain of an exact implementation with respect to our proposed method, should be carefully assessed, since it may only be marginal, and may not be worth the effort.

4. Results

In order to assess our proposal we have applied it to two processes, W production and top quark pair production. Besides being of considerable phenomenological significance in their own right, these processes represent a reasonably wide range testing ground; on the one

hand W production is a quark anti-quark annihilation process with a relatively low mass final-state, while on the other, $t\bar{t}$ pair production is predominantly gluon initiated with a high invariant mass final-state. Here our intention is to demonstrate the effectiveness of the MENLOPS approach and to give a more quantitative understanding of its domain of applicability. The analyses presented in this section are therefore carried out at the parton level, after parton showering, without applying acceptance cuts.

The following conventions are adopted throughout for the histograms:

- Dashes (red) - the pure NLOPS result
- Dots (green) - the pure MEPS result *rescaled* by a global K -factor: $\sigma_{\text{PW}}(\geq 0)/\sigma_{\text{ME}}(\geq 0)$
- Solid (blue) - the MENLOPS sample
- Dashes with “ \times ” symbols (red) - the NLOPS component of the MENLOPS result
- Dots with “ $+$ ” symbols (green) - the MEPS component of the MENLOPS result

Unless stated otherwise, in each plot the jet resolution scale is the same as the merging scale used to create the corresponding MENLOPS sample.

4.1 POWHEG and MEPS simulations

For both processes under study MEPS merged samples were generated using the MADGRAPH package [18]. This program employs the MLM merging scheme, with minor differences in the form of the cuts used for the generation of the tree level events, and in the use of the k_{\perp} -jet measure [24, 25], as opposed to a cone jet measure, to perform the parton-jet matching. The PYTHIA [26] virtuality ordered parton shower is used to simulate radiation from the external legs of the events generated according to tree-level matrix elements. This implementation is referred to as the k_{\perp} -jet MLM scheme in the documentation [27], a full account of which is given in Ref. [28].

NLOPS W and top-quark pair production events were simulated using the POWHEG-w [7] and POWHEG-hvq [6, 29] codes respectively, showering the output Les Houches event files with the same PYTHIA library included in MADGRAPH. In order to be completely faithful to the POWHEG formalism, in showering the events from the Les Houches files we have opted to use the transverse momentum ordered PYTHIA shower algorithm, setting the starting scale for each event to the value given in the Les Houches file, i.e. the transverse momentum of the hardest emission. Other types of shower algorithms, not ordered in transverse momentum, may be used, but care should then be taken to veto emissions which have a transverse momentum greater than that of the hardest in the input POWHEG event.

Although the NLOPS samples used in obtaining the final results were generated in complete adherence to the POWHEG formalism, we have also experimented with various combinations of shower orderings and starting scales. In all cases we found only small, inconsequential differences. In particular, we have repeated the following analyses using the

PYTHIA virtuality ordered shower algorithm, with the so-called *Herwig scale* as the initial condition, when showering POWHEG events. This scale is given by the invariant mass of the least massive pair of colour connected particles in the parton level event. Hence, this amounts to using the same MEPS showering apparatus for the NLOPS events. The differences seen with respect to the results shown here were marginal and of no interest. This is perhaps not surprising given that the pair of colour connected partons with the lowest invariant mass is generally that with the smallest relative transverse momentum, which in the POWHEG case is essentially always given by that of the radiated parton.

In choosing the tree level event generation parameters and the MEPS merging scale, we have closely followed the settings recommended in Refs. [16, 27, 28] for applying the k_{\perp} -jet MLM scheme to W boson and top quark pair production at LHC. In the event that an alternative value of a parameter was not advised, the default value in the MADGRAPH program was used.

Excepting the differences in the choice of shower algorithm used for the NLOPS and MEPS samples, we aimed to have the remaining inputs as consistent as possible in generating the two. In particular, we have used the same parton density functions in the POWHEG, MADGRAPH and PYTHIA programs, MRST 2002 NLO [30], provided in all cases through the LHAPDF interface [31]. In all programs the top quark and W boson masses have been duly set to 174.3 and 80.419 GeV; similarly, a value of 2.124 GeV was used for the width of the W boson. The default MADGRAPH input was also adjusted in order to include the contributions of b-quarks in the initial- and final-state, as in the POWHEG simulations. Finally, we have generated our event samples assuming the nominal LHC hadronic centre-of-mass energy, $\sqrt{s} = 14$ TeV.

The authors of Ref. [16] observe that the emission spectrum from the transverse momentum ordered shower tends to be markedly harder than that of the virtuality ordered shower, modulo differences in the starting scales. This enables the former to populate additional, higher p_T , regions of phase space which the latter fails to reach. It is argued on these grounds that this shower approximation therefore has a greater range of validity, justifying a higher value of the MEPS merging scale. We prefer to interpret this observation more cautiously. Naturally, by emitting radiation where previously there was none, the transverse momentum ordered shower will produce results in seemingly better agreement with exact tree level, resummed, MEPS predictions. This is nevertheless an approximation, merely a less conservative one than that obtained with the virtuality ordered shower, as evidenced by the uncertainties surrounding the starting scales [16]. Because of this reason, and since using higher scales for merging would result in an advantage for the application of our method, we opt to generate the MEPS sample with the virtuality ordered shower and the 30 GeV MEPS merging scale in the present work, in order not to diminish its value as proof of concept of our method.

4.2 MENLOPS implementation

We have realised the merging algorithm described in Section 2 by dividing each NLOPS and MEPS sample into three sub-samples: a sample containing events with no additional radiated jets, a sample containing events with one radiated jet and a third sample comprised

of events with greater than one jet. In the NLOPS case the latter sample is discarded, while in the MEPS case it is kept and instead the other two are deleted. The fraction of events in the final Menlops sample with no additional jets is given by the same fraction found in the NLOPS sample. The fraction of events with one additional jet in the MENLOPS sample is given by one minus this 0-jet fraction, multiplied by the ratio of the number of 1-jet events to the number with one or more jets in the MEPS sample.

The exact choice of jet measure used to divide up the samples is not particularly important beyond the requirement that it be infrared safe, to avoid degrading, or losing altogether, NLO accuracy. To obtain the results in this section we used the k_\perp -jet measure [24,25], as implemented in the FastJet jet finder package [32]. Specifically, the k_\perp separation between two final state particles i and j is defined to be

$$d_{ij} = \min(k_{\perp i}^2, k_{\perp j}^2) \Delta R_{ij}^2 / R, \quad (4.1)$$

with $\Delta R_{ij}^2 = (Y_i - Y_j)^2 + (\phi_i - \phi_j)^2$, where $k_{\perp i}$, Y_i and ϕ_i are the transverse momentum, rapidity and azimuth of particle i . The factor R is a jet-radius parameter which has been set equal to one in our analysis. In addition, in this scheme the *beam distance* is defined as $d_{iB} = k_{\perp i}^2$.

The MENLOPS merging scale according to which the MEPS and NLOPS are sorted into 0-, 1- and greater than 1-jet samples is defined as a cut in the k_\perp separation measure, that is $y_0 = \sqrt{d_{\text{cut}}}$ (see Sect. 3). In the following analyses we shall also present distributions of the differential jets rates, where we query each event to establish the threshold in $y_{nm} = \sqrt{d_{nm}}$ at which an n -jet event is resolved as an $m = n + 1$ -jet event.

4.3 W boson production

We now turn to discuss the results obtained using MENLOPS samples for the case of W^- boson production. We consider the case wherein the W decays to an electron and neutrino. Naturally, these leptons are excluded from the jet finding procedure. Hence, when no additional radiation occurs, the jet finding algorithm returns 0 jets.

To generate the MEPS sample with MADGRAPH we have used a k_\perp jet measure cut on the tree level event generation of 15 GeV and taken the MEPS merging scale to be 20 GeV. These are the values advocated for the generation of inclusive W production samples in Refs. [27, 28].

The default MENLOPS sample used to produce the results in this subsection was constructed by combining the NLOPS and MEPS samples with a merging scale of 25 GeV, only 5 GeV above the MEPS merging scale. The MENLOPS cross section is equal to that of the NLOPS event generation, 8150 pb, and the fraction of MEPS events in the total sample is 5%, safely within the recommended maximum fraction α_S . We also show some results obtained using a MENLOPS sample generated with a merging scale of 40 GeV, for comparison. For this higher merging scale the number of MEPS events in the MENLOPS sample is 2%.

4.3.1 Jet multiplicities

In Figures 1 and 2 are the fractions of events in each of the samples, for various values of the jet clustering scale (see Sect. 4.2). The solid (blue) histogram shows the results of this

analysis procedure to a MENLOPS sample constructed as described in Sect. 4.2 using the default W production merging scale 25 GeV. The corresponding results for the pure NLOPS and MEPS samples are shown in the dashed (red) and dotted (green) lines respectively.

These plots serve to emphasize the physics behind the 0- and 1-jet cross sections as written in Sect. 2. Were it not for the formal technical difference between the jet measure and the k_T evolution variable, Eqs. (3.2) and (3.3) could be rewritten as

$$d\sigma_{PW}(0) = \overline{B}(\Phi_B) \Delta_R(y) d\Phi_B \quad d\sigma_{ME}(0) = \overline{B}_{ME}(\Phi_B) \Delta_{\hat{R}}(y) d\Phi_B, \quad (4.2)$$

where the Sudakov form factors here correspond to the probability that no emission occurs in the hard region $y > y_0$. The appearance of the 0-jet fraction histogram is then no surprise, having the characteristic Sudakov form factor shape.

One also can see the characteristic Sudakov form factor shape in the conditional 1-jet rate from the subsample of events with at least one jet. We remind the reader that this basically represents the probability for a 1-jet event to remain resolved as a 1-jet event, in evolving down from larger values of y . We see that in the pure NLOPS case this relative rate is significantly higher. This is a clear signal that additional jets are missing from the NLOPS simulation. These structures are as expected according to the arguments in Sect. 3 and the analysis surrounding Eqs. 3.1-3.4.

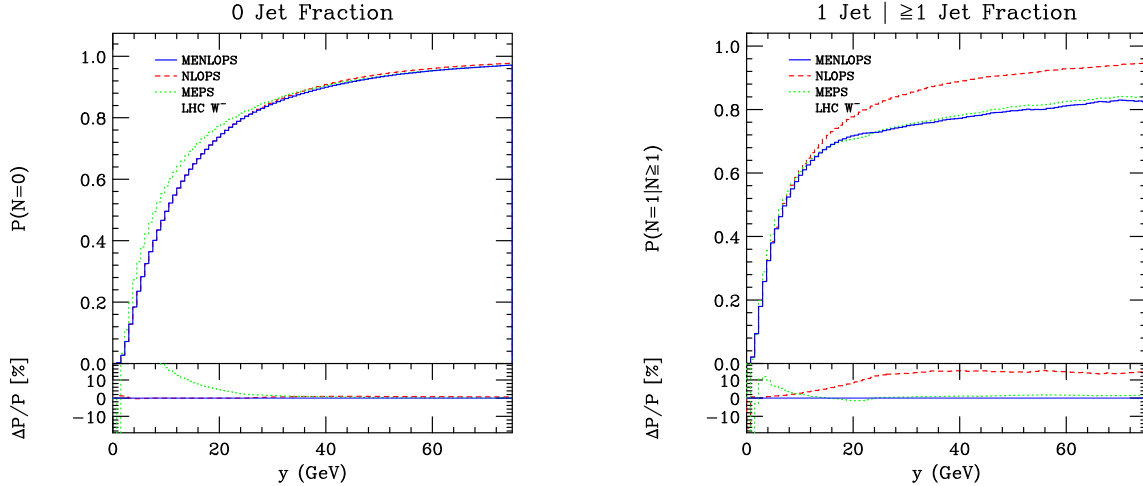


Figure 1: In the left plot, the dashed (red), dotted (green) and solid (blue) lines show the 0-jet fractions in the NLOPS, MEPS and MENLOPS $pp \rightarrow W^- \rightarrow \bar{\nu}_e e^-$ samples respectively, as a function of the jet resolution scale y , defined according to the Durham k_\perp jet measure. On the right plot, the number of 1-jet events over the total number of events with at least one jet is reported.

The full 1-jet fraction in Fig. 2 is a combination of the complement to 1 of the 0-jet fraction and of the conditional one jet fraction (i.e. it is one minus the left plot times the right plot in Fig. 1).

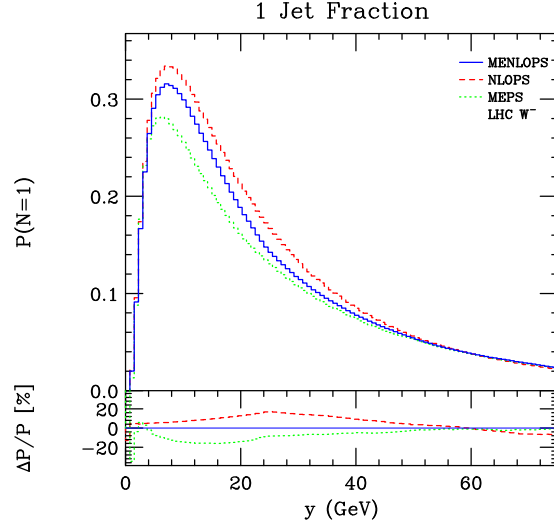


Figure 2: The fraction of 1-jet events of the NLOPS, MEPS and MENLOPS full samples, as a function of the jet clustering scale y . The convention for the line types (and colours) are the same as in the previous plots.

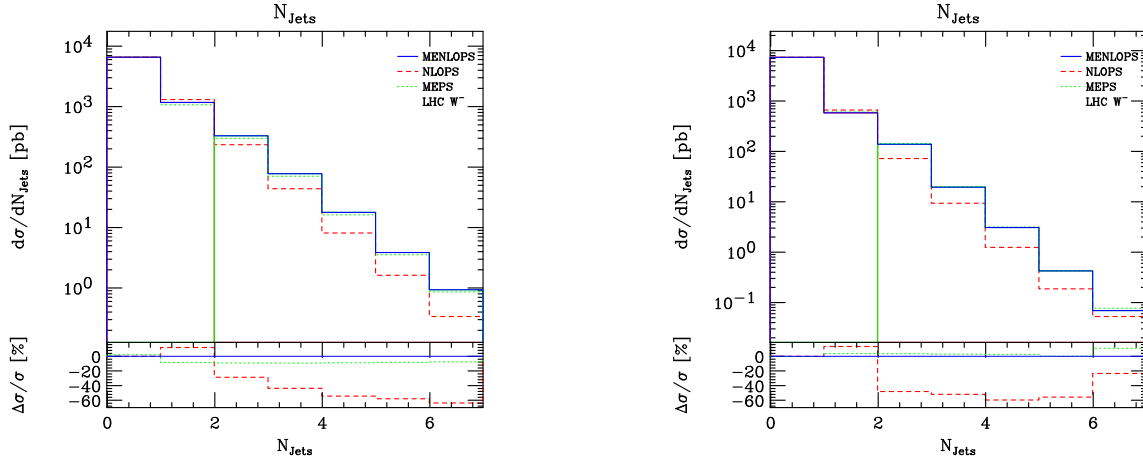


Figure 3: The jet multiplicity distributions for $W^- \rightarrow e^- \bar{\nu}_e$ using two different choices of the MENLOPS merging scale: 25 GeV (left) and 40 GeV (right).

Looking at the 0-jet fractions in Fig.1 one sees that there is a tendency for the MEPS sample to contain fractionally more soft events than the other two. This may be understood as being due to differing approaches to the soft resummation in the POWHEG simulation, with respect to the PYTHIA virtuality ordered shower. The description of the soft region obtained from the transverse momentum ordered shower is theoretically much closer to that in POWHEG, producing results in much better agreement in that region. We hasten to add that the choice of scales used in the evaluation of the PDFs in the transverse momentum ordered shower is also theoretically more sound [5, 33]. However, from the point of view of the MEPS merging aspect, on the whole we have found better results with the virtuality

ordered shower, for which the MADGRAPH MLM implementation is more mature. Also we favor maximizing the corrective effects which arise from the exact matrix elements. With this in mind the virtuality ordered description is preferable since it allows a lower value of the MEPS merging scale.

Turning to the 1-jet fractions the picture is somewhat different. Here the fraction of 1-jet events, in the soft region, is around 20% lower in the MEPS and MENLOPS samples, for larger values of the clustering scale. This is indicative of the fact that the fraction of events with more than one jet, with respect to the fraction with at least one jet, is higher in the MEPS sample, through the inclusion of $\mathcal{O}(\alpha_S^2)$ tree level matrix elements².

At this point we feel it may be useful to put these figures in context with regard to the MENLOPS algorithm and the theoretical arguments surrounding it in Sect. 3. Specifically, recall that in POWHEG, for small values of the clustering scale, the distribution of radiation in the 0-jet sample is dominated by large logarithms (Eqs. 3.1,4.2) and is therefore, formally, no worse in accuracy than any parton shower. Conversely, at higher values of the clustering scale the large logarithms are suppressed and the full NLO accuracy of the POWHEG simulation therefore gives a much better prediction. From the 0-jet fraction plot one can see that the MENLOPS sample is combined, from the point of view of the cross section, at a high value of the clustering scale, with 80% of events containing no extra jet activity. In any case, the 0-jet cross section, which plays a key role in determining the content of the MENLOPS sample, is *always* described by the NLOPS prediction at least as well as the MEPS one; the MENLOPS sample contains the same fraction of 0-jet events as the NLOPS one by design.

Displayed in Figure 3 are the jet multiplicity distributions obtained by merging the NLOPS and MEPS samples with MENLOPS merging scales of 25 GeV and 40 GeV, using the same scale to define the jets in each case. Here one sees that the cross section for lower jet multiplicities is larger in the sample with the 40 GeV merging scale than in the 25 GeV one, while the opposite is true for the higher multiplicities. The nature of the results shown here can be easily explained. The gap between the pure MEPS and MENLOPS results, as seen in the fractional difference plots, is small, indicating that the K -factor for the total cross section is in close agreement with the K -factor associated with the production of at least one jet. This can also be understood by considering that the size of the gap is proportional to, amongst other things, the difference in the 0-jet fractions, which can be seen to vanish at 40 GeV in Figure 1.

4.3.2 Inclusive observables

In Figure 4 we show the transverse momentum spectrum of the e^- from the W^- decay, as well as the rapidity of the W^- , for two different choices of the MENLOPS merging scale, our default value of 25 GeV and also 40 GeV. In respect of these quantities there are two main points to consider: the stability and composition of the MENLOPS sample with respect to changing the merging scale, and also potential differences due to NLO effects.

²Note that the inclusion of the higher order tree level matrix elements can equally lead to a *reduction* in the 1-jet fraction with respect to that in the shower approximation.

In all cases these inclusive MENLOPS predictions are shown to be insensitive to the change in the merging scale. We draw attention to the fact that the high p_T tail of the electron transverse momentum spectrum, for the 25 GeV scale choice, is entirely due to events from the MEPS sample, *i.e.* events with at least two jets, while for the 40 GeV choice it is given by an even mixture of MEPS and NLOPS events. The stability of the result follows from the fact that the two types of simulation are in good agreement regarding the shapes of this distribution.

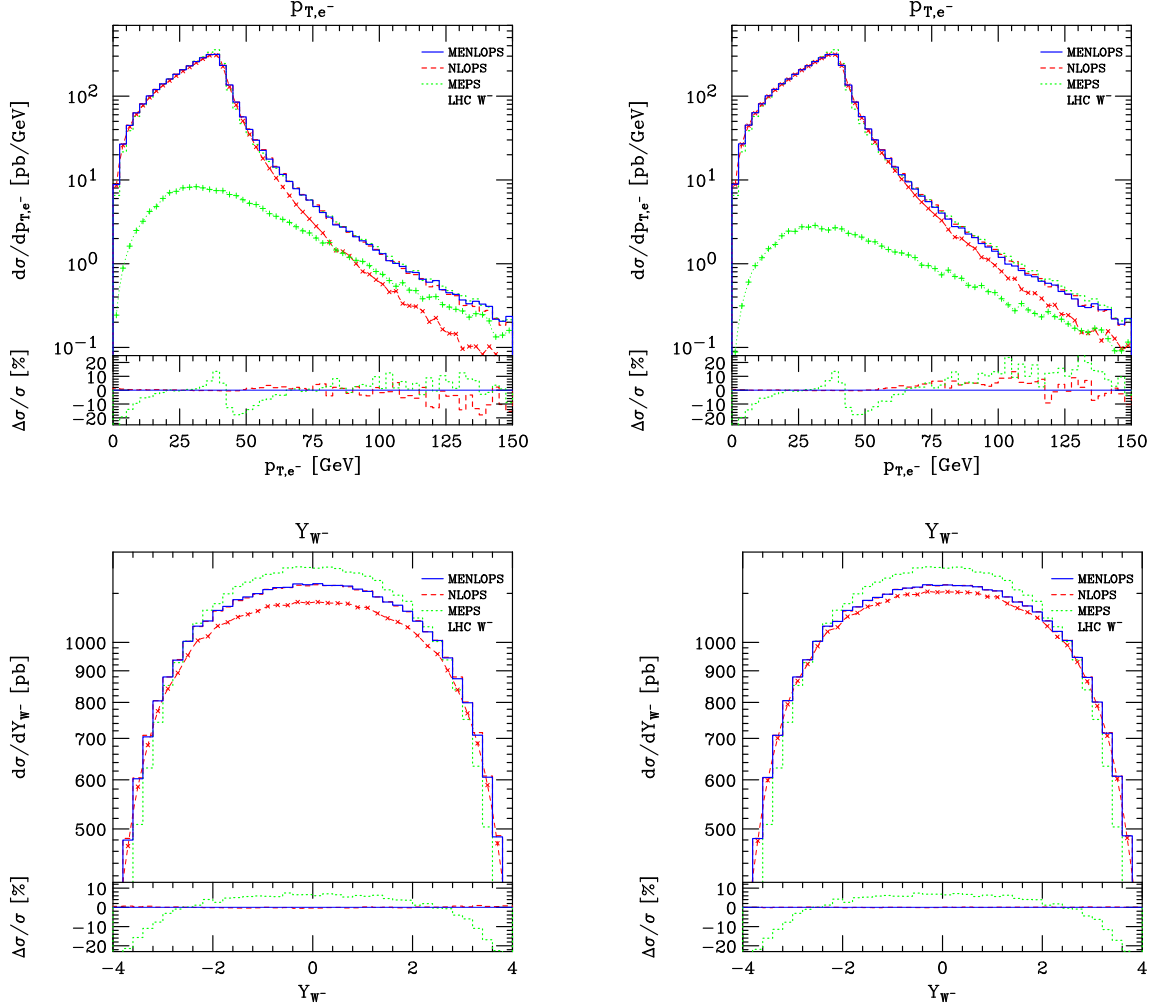


Figure 4: In the upper half of this figure we show the transverse momentum of the electron in $W^- \rightarrow e^- \bar{\nu}_e$ using a 25 GeV (left) and 40 GeV (right) jet resolution scale in performing the MENLOPS merging. The lower pair of plots shows, analogously, the rapidity distribution of the W^- . Despite the relatively large difference in the merging scales the combined MENLOPS prediction is stable with respect to the changing scale, showing deviations from the NLO result at the level of only 1 or 2% in both cases.

The distribution for the rapidity of the W^- is also interesting. Here again we see that the distribution is stable with respect to changing the MENLOPS merging scale from 25 to 40 GeV, and in both cases only exhibits $\mathcal{O}(1\%)$ level fluctuations with respect to the NLOPS

prediction. This behavior is rather unsurprising, since the MEPS contribution constitutes no more than 5% of the total number of events in the MENLOPS sample for the case of 25 GeV merging scale and hence even less for the 40 GeV case.

Note that the shape of the MEPS and NLOPS/MENLOPS rapidity spectra show rather large differences, up to 20%. Such differences can occur through the use of different PDFs. However, in our case, the MRST 2002 NLO parton density functions were used in all aspects of the generation process. Inconsistencies in the treatment of the CKM matrix and proton flavour content could also cause some discrepancies. However we have checked that the inputs to the MEPS and NLOPS simulations are compatible in this respect; b -quarks are included in both cases and the V_{ud} CKM matrix element is set to 0.975 (differences due to the last two factors should in any case be very small; in fact, we found that using a diagonal CKM matrix has a completely negligible effect on distributions).

Intuitively one might expect that the addition of multiple hard jets to a leading order parton shower simulation, as in the MEPS case, would require the produced system, and thus also the W , to be more central. Exactly this behavior can be seen in, for example, Figure 3 of Ref. [34], where it is clear that the pseudorapidity of the Z boson in the Drell-Yan process is less central when only the leading order matrix element is used in generating the MEPS sample. This is in line with the differences we see in the rapidity distributions in Figure 4. For this observable, the results in Ref. [34] only have leading order accuracy, meaning that the effect witnessed there is beyond the remit of that study and is duly neglected there. In the context of our theoretical analysis in Section 2, this effect is contained in the ratio of $\overline{B}_{ME}(\Phi_B)/B(\Phi_B)$. Hence we conclude that the differences may be attributed to the inclusion of NLO terms in the NLOPS/MENLOPS samples that are not present in the MEPS one. This conclusion is supported by the result displayed in Fig. 13 of Ref. [7], where it is shown that, if the same parton densities are used, there is no difference in the shape of the LO and NLO rapidity distribution of the vector boson. This means that the effect of real corrections, that would make the distribution more central, are exactly compensated by NLO virtual effects.

We now turn our attention to the W boson p_T spectra seen in Figure 5. We observe that the distribution is essentially stable with respect to the change in MENLOPS merging scale, from 60 to 100 GeV, with the MENLOPS prediction being indistinguishable from the NLOPS one. This again reflects the good agreement in the shape of the MEPS and NLOPS predictions since the latter dominate the MENLOPS sample in the region above 75 GeV in the default sample.

We ascribe the increasing MEPS content of the MENLOPS sample, at high p_T , as being due to the fact that such events naturally involve more energy transfer, and therefore they should be associated with more jet activity. More technically, consider that if a high transverse momentum W boson is observed, momentum conservation requires that there be an equally significant amount of momentum in the form of QCD radiation to balance it. From our earlier expressions for the 1-jet cross section Eq. 3.4 one can deduce that the probability for a 1-jet event, with the jet produced at some high scale p_T , to remain resolved as a 1-jet event at the lower scale y_0 , is given by the effective Sudakov form factor for that configuration. It follows that the higher is the initial value of p_T , the less likely one is to

still observe just one jet at y_0 . This argument is of course rather general and the structure of the MENLOPS predictions for all of the p_T spectra in these results can be understood in these terms.

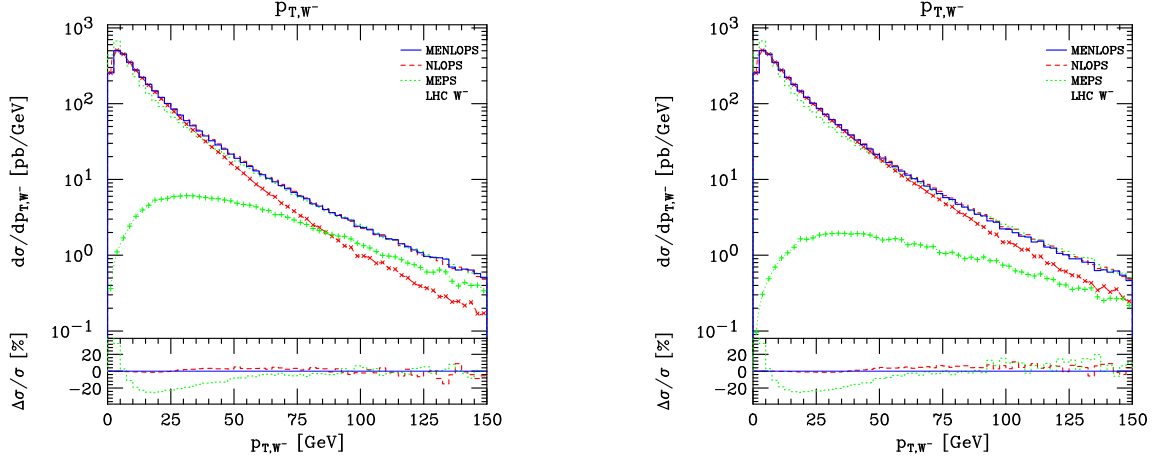


Figure 5: The transverse momentum spectrum of the W^- using a 25 GeV (left) and 40 GeV (right) jet resolution scale as the MENLOPS merging scale. As in Figure 4, the greater resolution scale used in producing the MENLOPS sample (solid) on the right hand side results in the MEPS component (dotted) being greatly diminished. Nevertheless, the merged distribution very much assumes the form of the pure NLOPS prediction (dashed) to within $\mathcal{O}(1\%)$, with deviations only beginning to become noticeable in the high p_T tail, where contributions from events containing more than one jet become more important.

4.3.3 Jet activity

In Figure 6 we show the transverse momentum and rapidity distributions of the first and second highest p_T jets in $pp \rightarrow W(\rightarrow e^- \bar{\nu}_e) + \text{jets}$. The distributions for the leading jet mirror the corresponding ones for the W^- boson which it recoils against. The composition of the MENLOPS p_T spectrum result can be understood in much the same way as was just discussed for the case of the W^- boson p_T , with one key difference being the degree of exclusivity of the observable. Whereas the W^- transverse momentum includes contributions from all jet multiplicities, and is therefore predominantly based on 0-jet NLOPS events, the leading jet p_T spectrum, obviously, includes no contributions from 0-jet events. Hence, a greater fraction of events with at least two jets (MEPS events) enter this prediction. This explains why, in the high p_T region, the MENLOPS prediction for the W^- transverse momentum spectrum is equal to that of the NLOPS sample, while for the leading jet it is instead equal to the MEPS one.

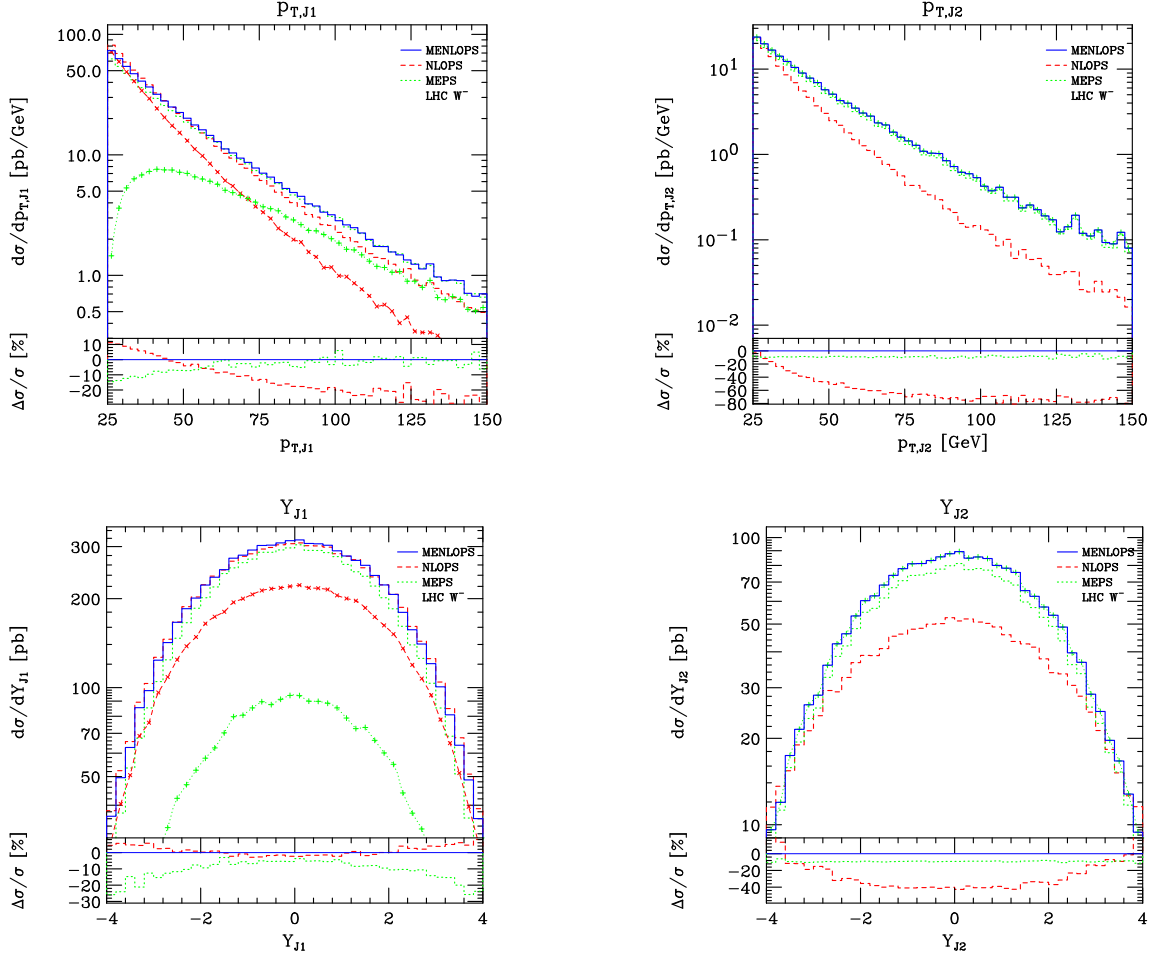


Figure 6: In the upper half of this figure we show the transverse momentum distribution of the hardest (left) and second hardest (right) jets, with the corresponding rapidity distributions shown underneath. The MENLOPS predictions (solid) shown here and their NLOPS (dashed) and MEPS (dotted) components were obtained from a MEPS-NLOPS combination with a merging scale of 25 GeV.

The fact that the MEPS and NLOPS results are different by 25% in this tail region is an entirely separate issue. We iterate that, formally, both MEPS and NLOPS simulations are only capable of describing predictions for the leading jet with leading order, leading-log, accuracy. With this in mind the difference seen is basically of higher order in α_S . Having said that, we note that the MEPS result tends to overestimate the NLOPS one.

Finally, we remark that it may seem puzzling that the MEPS and NLOPS results agree very well for the W^- transverse momentum spectrum and yet not so well for that of the leading jet. This is explainable by considering that the NLOPS simulation will prefer to produce additional radiation in the shower approximation, in the direction of the leading jet or of the incoming beams, whereas the MEPS simulation is more capable of producing additional radiation closer in angle to the W^- boson, thus requiring the leading jet to recoil more.

The predictions for the second jet are completely determined, by construction, by the

MEPS sample. The corrective effects of the MEPS contributions in the jet rapidity distributions have a more intuitive understanding; since the second hardest jet in the POWHEG simulation originates from the parton shower, the subset of two jet events generated in this way will tend to have proportionally more events in which the second jet is more collinear with the beam axis, than in the MEPS case.

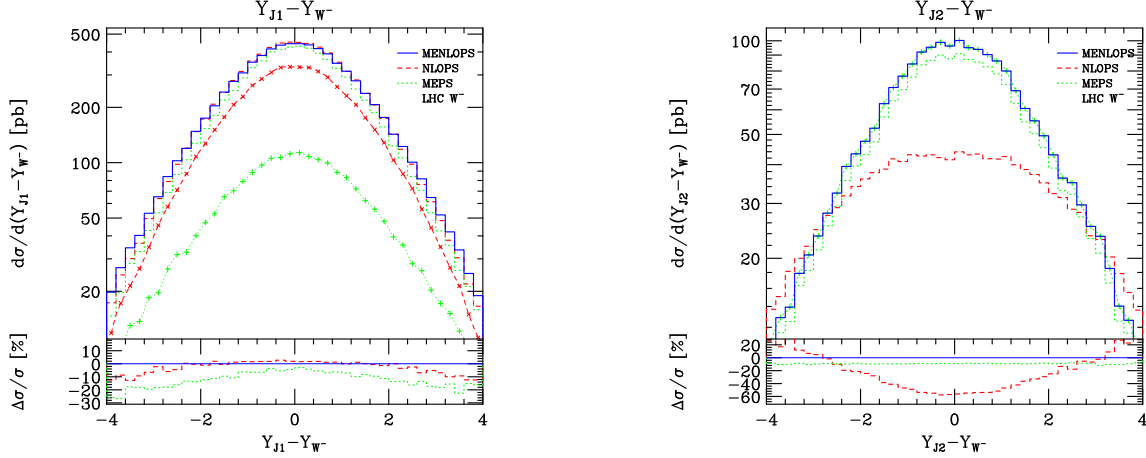


Figure 7: In this figure we show the rapidity difference between hardest jet and W^- boson (left) and the second hardest jet and the W^- boson (right). The first plot requires the presence of at least one jet in the event, precluding contributions from 0-jet NLOPS events. Hence, the relative MEPS component of the MENLOPS sample (solid green) is increased with respect to the case of the W^- rapidity distribution (Fig. 4). In the other plot the MENLOPS sample comprises of only MEPS events and a considerable correction to the NLOPS result can be seen. This correction is due to the fact that the parton shower approximation is used to generate jets beyond the leading jet in the NLOPS simulation, whereas the MEPS result is better, giving a leading order prediction for this distribution.

Substantial improvements in the description of the second jet can be seen again very clearly in Figures 7 and 8. Figure 7 shows a correction of 60% in the MEPS/MENLOPS predictions with respect to the NLOPS result in the rapidity of the second jet with respect to the W^- boson. The second jet in the MEPS and MENLOPS samples is significantly more central than in the NLOPS case, which is probably due to the fact that the MEPS approach is more likely to produce central jets than the shower algorithm.

Similarly large corrections can be seen in the azimuthal correlations shown in Figure 8. On account of the fact that the second hardest jet in the NLOPS approach originates from the shower approximation, any additional radiation from the incoming legs is essentially distributed uniformly in azimuth, while final state radiation is strongly correlated with the direction of the leading jet. Given this fact one expects a deficit of events in the NLOPS sample for which the difference in azimuth between the W^- and the leading jet, $\Delta\phi_{J1,W^-}$, is small. This is indeed seen to be the case in Fig. 8, which reveals that the deficit is a rather significant one. A similar trend can be seen later, for the case of $t\bar{t}$ pair production, concerning the $\Delta\phi_{J1,t\bar{t}}$ correlation (Fig. 16).

Figure 8 also shows the azimuthal correlation between the two leading jets. The MEPS

and MENLOPS predictions exhibit a much higher degree of correlation in the back-to-back region. In the NLOPS simulation the only correlations which may be present there are those due to kinematics and momentum recoil effects, as opposed to genuine dynamics, since the shower Monte Carlo produces secondary radiation that either follows the direction of the leading jet (and thus has small azimuth), or is emitted by the incoming partons, and is thus uniform in azimuth.

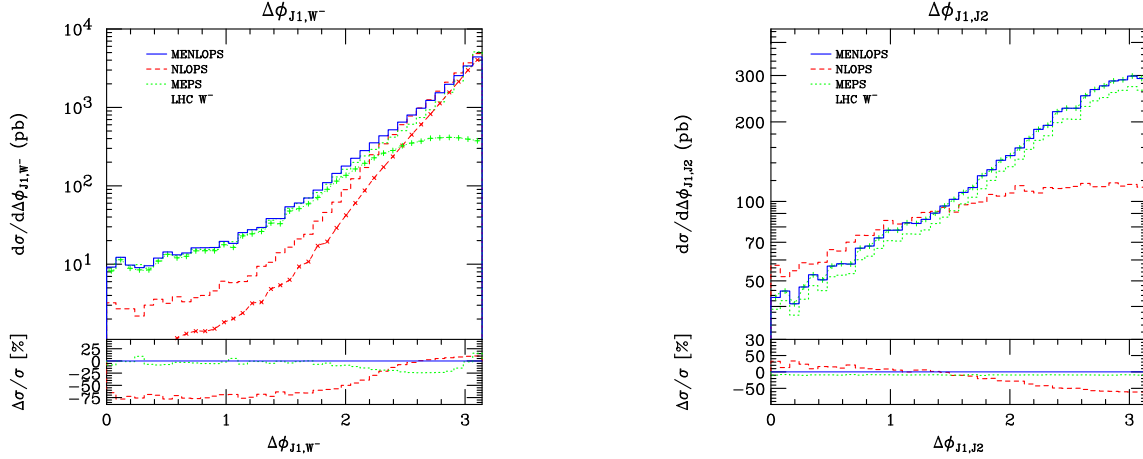


Figure 8: In this figure we show two distributions further illustrating how the description of additional jet activity compares in the NLOPS, MEPS and MENLOPS event samples. On the left we show the difference in azimuth between the leading jet and the W^- boson, while on the right we show the difference in azimuth between the two leading jets. These distributions show large differences by virtue of the fact that the description of the second jet in the NLOPS simulation is given by the parton shower approximation. The parton shower approximation strictly only contains information on the collinear limits of matrix elements and, furthermore, it does not propagate spin correlation information along the shower.

Lastly we consider the differential jet rates displayed in Figure 9. Recall that these distributions directly probe the behavior of the MEPS and MENLOPS samples around the phase space partitions in these two approaches. We recall that the merging scale used to make the MEPS combination was taken to be 20 GeV, while in making the default MENLOPS sample we use a value of 25 GeV.

In the MEPS case the merging between the parton shower and the matrix elements involves a phase space partition for every different multiplicity. In the MENLOPS case all events with 0 or 1 jet are described by the one NLOPS simulation, with the MEPS sample alone describing the rest. It follows that the MENLOPS approach should not induce the appearance of discontinuities in the differential jet rates, with the exception of the y_{12} jet rate, where there is a complete transition at 25 GeV from the MEPS description to the NLOPS one.

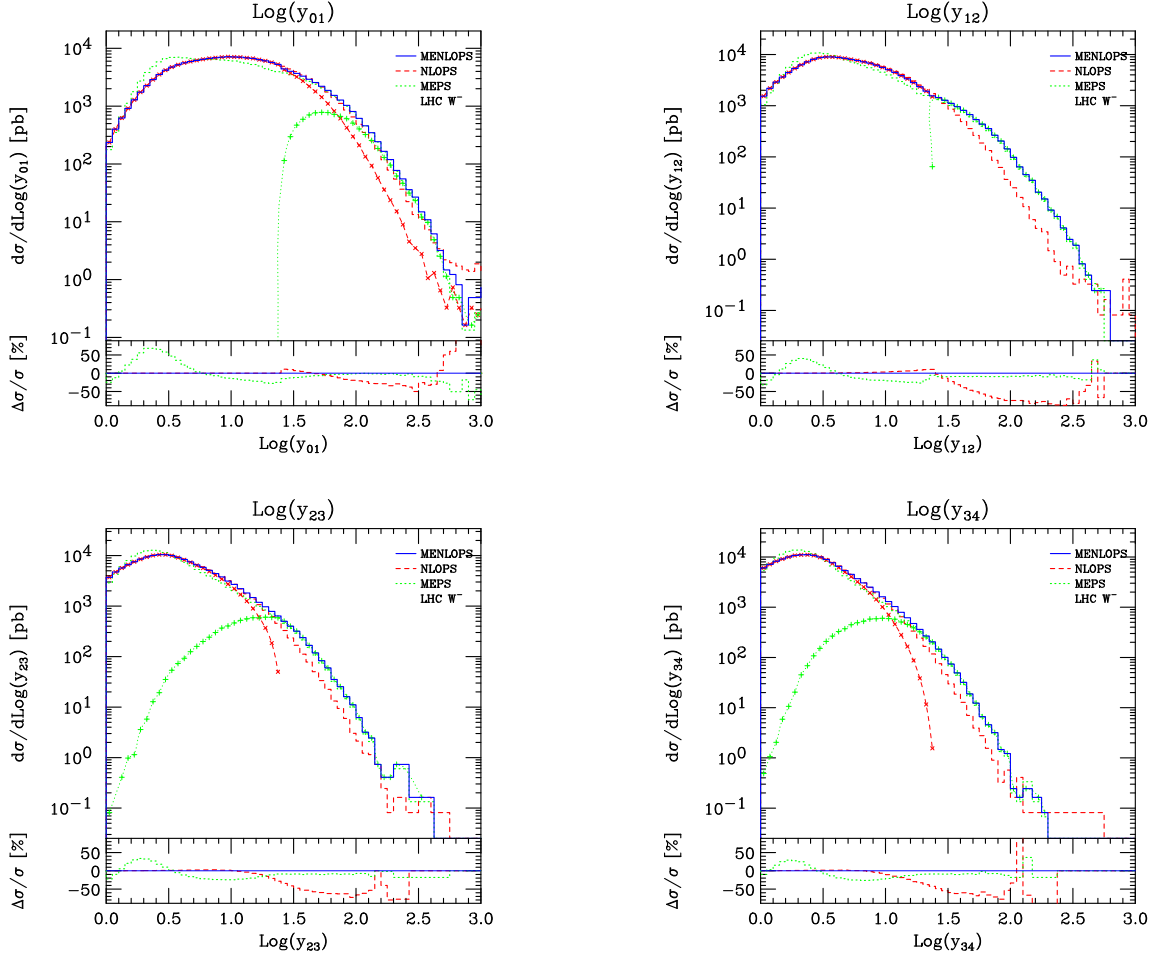


Figure 9: Differential jet rates for $pp \rightarrow W^- (\rightarrow e^- \bar{\nu}_e) + \text{jets}$. These plots show the logarithm of the value of the jet clustering scale y_{nm} at which an n -jet event is resolved as an $m = n + 1$ -jet event.

In all cases one can see that the predictions from the pure MEPS sample (green dots) are smooth with no evidence of any merging scale dependence. The two distributions exhibit some differences in the soft region, the MEPS sample favoring more soft emission. This behavior has already been noted in the discussion of the 0-jet fraction in Fig. 1, where it was attributed to differences in the MEPS Sudakov form factors with respect to POWHEG.

The MENLOPS predictions (blue) are also smooth across the 25 GeV boundary in the y_{12} distribution, in spite of the abrupt transition from the NLOPS to the MEPS samples. Some relatively minor distortion in the first derivative can be seen at this point in the y_{12} plot. However, it is similar in magnitude to that seen in the pure MEPS results.

In general one should not expect that either the MENLOPS or the MEPS differential jet rates be completely smooth, since the distributions either side of the boundary are only formally equivalent at the leading-log level, differences by terms of $\mathcal{O}(\alpha_s)$ should be expected in both cases. However, since in both procedures one aims to merge at the lowest scale allowed the large logarithms dominate the distributions at the merging partition(s).

In principle there is no reason why one may not construct the MENLOPS sample using a *floating* value of the merging scale. In fact it is testament to the flexibility and transparency of the whole approach that this floating scale can be implemented with great ease, in dividing the MEPS and NLOPS samples. We have also performed such a merging taking the scale to be Gaussian distributed about 25 GeV with a standard deviation of 5 GeV. The results of doing this are the same as above, although the y_{12} jet rate naturally appears smoother this way. However, we prefer to be prudent and present our results in such a way as to be open about the presence of the unphysical scale.

4.4 Top quark pair production

In this subsection we present the results of applying our method to the top quark pair production process. The simulation of the top quarks in both MEPS and NLOPS samples does not include their decay. In addition, the final-state top quarks are not input to the jet clustering process; thus when no additional radiation occurs the jet finding algorithm will return 0 jets.

In producing the MEPS sample with MADGRAPH we have set the k_{\perp} jet measure cut on the tree level event generation to be 20 GeV, and we have chosen the corresponding MEPS merging scale to be 30 GeV. These values are recommended for the production of inclusive $t\bar{t}$ pair production in Refs. [16, 27], when using the virtuality ordered PYTHIA parton shower. We note that the recommended MEPS merging scale in the case of the transverse momentum ordered shower is 100 GeV, much larger than our chosen value.

The default MENLOPS sample used to produce the results in this subsection was constructed by combining the NLOPS and MEPS samples with a merging scale of 60 GeV. This scale is 30 GeV above the merging scale in our MEPS sample but still lower than that recommended in the case of merging with the transverse momentum ordered shower [16]. The MENLOPS cross section is equal to that of the NLOPS event generation, 817 pb, and the fraction of MEPS events in the total sample is 12.5%, marginally above α_S . In looking at the jet multiplicity distributions and inclusive observables it is useful to consider the effects of varying the merging scale, hence, some results are also obtained using a greater merging scale of 100 GeV, for which the fraction of MEPS events in the MENLOPS sample drops to 4%.

As explained in Section 2, and as will be demonstrated in the following, the fraction α_S of MEPS events in the sample has a completely negligible impact on the NLO accuracy of inclusive observables. However, to lower the merging scale further will lead to an increased number of MEPS events and formally compromise NLO accuracy. Hence the MENLOPS description here can be understood as offering the best of the NLOPS and MEPS descriptions except, arguably, in the k_{\perp} -jet measure window $30 < y_{ij} < 60$ GeV, for jet multiplicities higher than two, which is populated by events taken from the NLOPS sample.

4.4.1 Jet multiplicities

Shown in Figures 10 and 11 are the 0- and 1-jet fractions in each of the samples, as a function of our jet resolution parameter y (Sect. 4.2). These histograms were made by applying the exclusive jet finding algorithm to each of the samples at different values of

the clustering cut parameter. The solid (blue) histogram shows the results of this analysis procedure when applied to a MENLOPS sample constructed as described in Sect. 4.2 with a merging scale of 60 GeV, the corresponding results for the pure NLOPS and MEPS samples are shown in the dashed (red) and dotted (green) lines respectively. The 0-jet fraction has the typical shape of a Sudakov form factor. This is in keeping with the fact that the latter has an interpretation as the probability for not emitting any radiation above a given scale. We also show for each sample the conditional probability for obtaining a 1-jet event from a sample of events where each contains at least one jet. The ratio of the latter quantity in the MEPS and NLOPS samples is used in constructing the MENLOPS sample Eq. 3.6. Using similar reasoning to that above, this quantity can be thought of as representing the Sudakov form factor probability for a 1-jet event to evolve into a ≥ 2 -jet event at the given scale. As with the 0- and 1-jet distributions this Sudakov form factor should be understood in the sense of having been averaged over the underlying Born variables. This is clear from the form of the distribution in Figure 10. The 1-jet fraction of Figure 11 results from the combined effects of the Sudakov form factor for 0-jet emission, that differs from 1 by the probability to emit 1 or more jets, and the probability to find a 1-jet event out of the sample of events with at least one jet.

Having elaborated on the general dynamics behind the jet fractions, we now move to discuss the finer details of the distributions, comparing the predictions from each merging scheme. It is clear from the plots that the largest differences between the NLOPS and MEPS samples occur in the region of the Sudakov peak, where the rates are governed by the all orders resummation of large logarithms. In the case of the 0- and 1-jet fractions, below the MEPS merging scale (30 GeV), this is therefore the difference between the PYTHIA virtuality ordered parton shower and the POWHEG hard emission generator. Since the resummation in the POWHEG case is nearly NLL accurate, this quantity is better determined by it than by PYTHIA. In fact, as we will discuss in more detail later in the context of the $t\bar{t}$ p_T spectrum, the POWHEG prediction offers a substantial improvement over that of the virtuality ordered shower from the point of view of the treatment of the scales used in the evaluation of the PDFs. Note that below the MENLOPS merging scale (60 GeV) the 0-jet fraction in the MENLOPS sample is identical, by construction, to the NLOPS result, while in the case of the 1-jet fraction they are different by a constant factor (see Eq. 3.6).

Going above the 60 GeV merging scale, as we resolve the events over increasingly large y values, one sees that the MENLOPS 0- and 1-jet fractions begin to include proportionally more MEPS events, since, for example, 2-jet events at the MENLOPS merging scale are resolved as 0- and 1-jet events at these higher scales. Also, above the 60 GeV merging scale, the conditional probability for obtaining a 1-jet event given a set of events each with at least 1-jet, is by default equal to that in the MEPS sample. Recall that this is very closely related to the Sudakov form factor probability for a 1-jet event to evolve to a scale below the jet resolution scale, without emitting any radiation. In the NLOPS case this is given by PYTHIA alone, while in the MEPS case corrections from exact, higher multiplicity, tree level matrix elements are included. Whereas, for small values of y , these probabilities are controlled by the Sudakov form factors in PYTHIA and in the MEPS, and thus the NLOPS and the MEPS have the same accuracy, for relatively large y the MEPS value should be

preferred, since it relies upon the exact matrix element result. This is why the MEPS value of this fraction is adopted in our MENLOPS method.

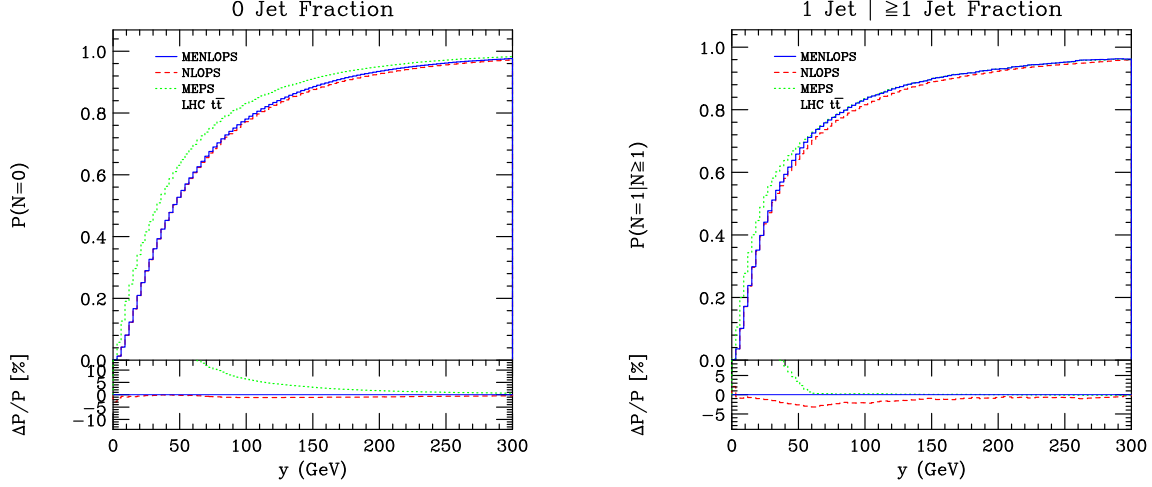


Figure 10: In the left plot we show the 0-jet fractions in the event samples, as a function of the jet resolution scale y , defined according to the Durham k_{\perp} jet measure. The dashed (red) and dotted (green) lines correspond to the pure NLOPS and MEPS predictions respectively. On the right plot we show the fraction of 1-jet events in the subset consisting of events with at least one jet.

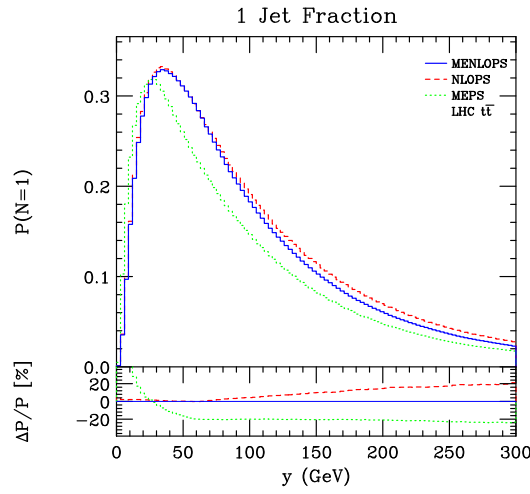


Figure 11: The 1-jet fractions in the event samples, as a function of the jet resolution scale y , defined according to the Durham k_{\perp} jet measure. The dashed (red) and dotted (green) lines correspond to the pure NLOPS and MEPS predictions respectively.

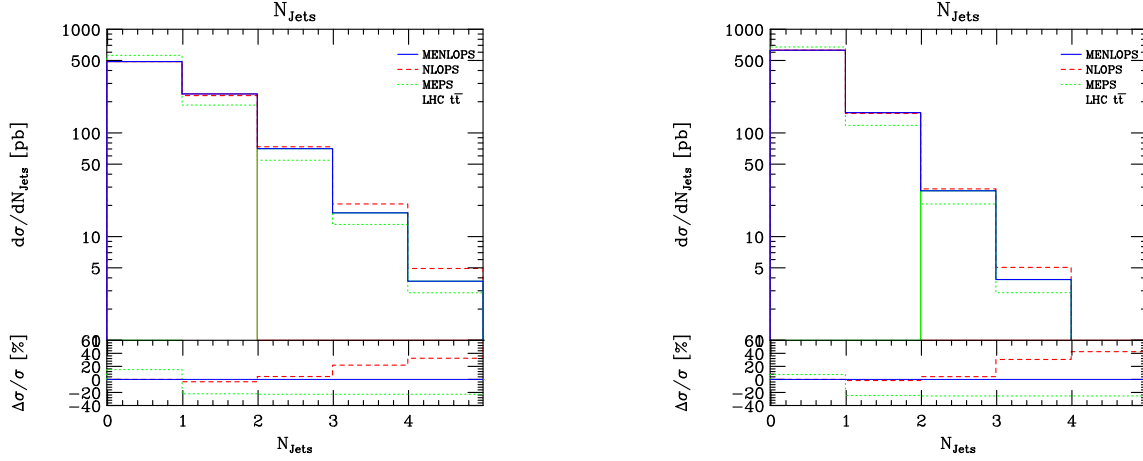


Figure 12: The jet multiplicity distributions for $t\bar{t}$ pair production events using two different choices of the MENLOPS merging scale: 60 GeV (left) and 100 GeV (right). In both cases we have used this merging scale as the jet resolution parameter in order to calculate the multiplicities. The 0- and 1-jet events in the MENLOPS sample are taken solely from the NLOPS sample, while those with higher multiplicities come from the MEPS one.

Figure 12 is meant to illustrate the working of the merging procedure. It shows the jet multiplicity distributions when the NLOPS and MEPS samples are combined with MENLOPS merging scales of 60 GeV and 100 GeV, with the jet resolution scale taken equal to the MENLOPS merging scale. As expected, one sees that the cross section for each value of the multiplicity is lower in the latter case.

Since the jet resolution scale here is equal to the MENLOPS merging scale, the MENLOPS histogram entry (solid) corresponding to events with no additional jets, as well as that of its NLOPS component, is exactly equal, by construction, to the pure NLOPS result (dashes). Equally, for jet multiplicities greater than one, the overall MENLOPS rates are exactly equal to those of the MEPS distribution (dots) multiplied by the NLO K -factor associated with the production of at least one jet, $\sigma_{\text{PW}}(\geq 1)/\sigma_{\text{ME}}(\geq 1)$, as described in Section 3 (Eq. 3.6).

These observations are most obvious from the ratio plots showing the fractional difference of the pure MEPS and NLOPS samples with respect to the MENLOPS one. We remind the reader that the pure MEPS prediction has been rescaled by a different K -factor, $\sigma_{\text{PW}}(\geq 0)/\sigma_{\text{ME}}(\geq 0)$, the ratio of the total cross sections. It follows that the dotted (green) line in the lower panels is constant with respect to the blue MENLOPS reference line, but not equal to it, the gap being given by the total K -factor divided by the K -factor for the production of at least one jet, minus one.

4.4.2 Inclusive observables

In Figure 13 we show the transverse momentum distribution of the top quark in $t\bar{t}$ pair production as well as the rapidity of the top quark pair, using two different scales to carry out the merging of the MEPS and NLOPS samples (60 GeV and 100 GeV).

The MENLOPS results are found to be blind to the variation in this unphysical merging scale, exhibiting no discernible deviation from the pure NLOPS result. This is particularly evident from considering the tail of the top quark p_T distributions. These observations are reassuring and completely understandable given the total content of the MENLOPS sample; for the 60 GeV merging scale the MEPS subsample comprises only 12.5% of the total, while in the 100 GeV case it is only 4%, therefore deviations from the pure NLOPS result are restricted to be of order 10% times α_S .

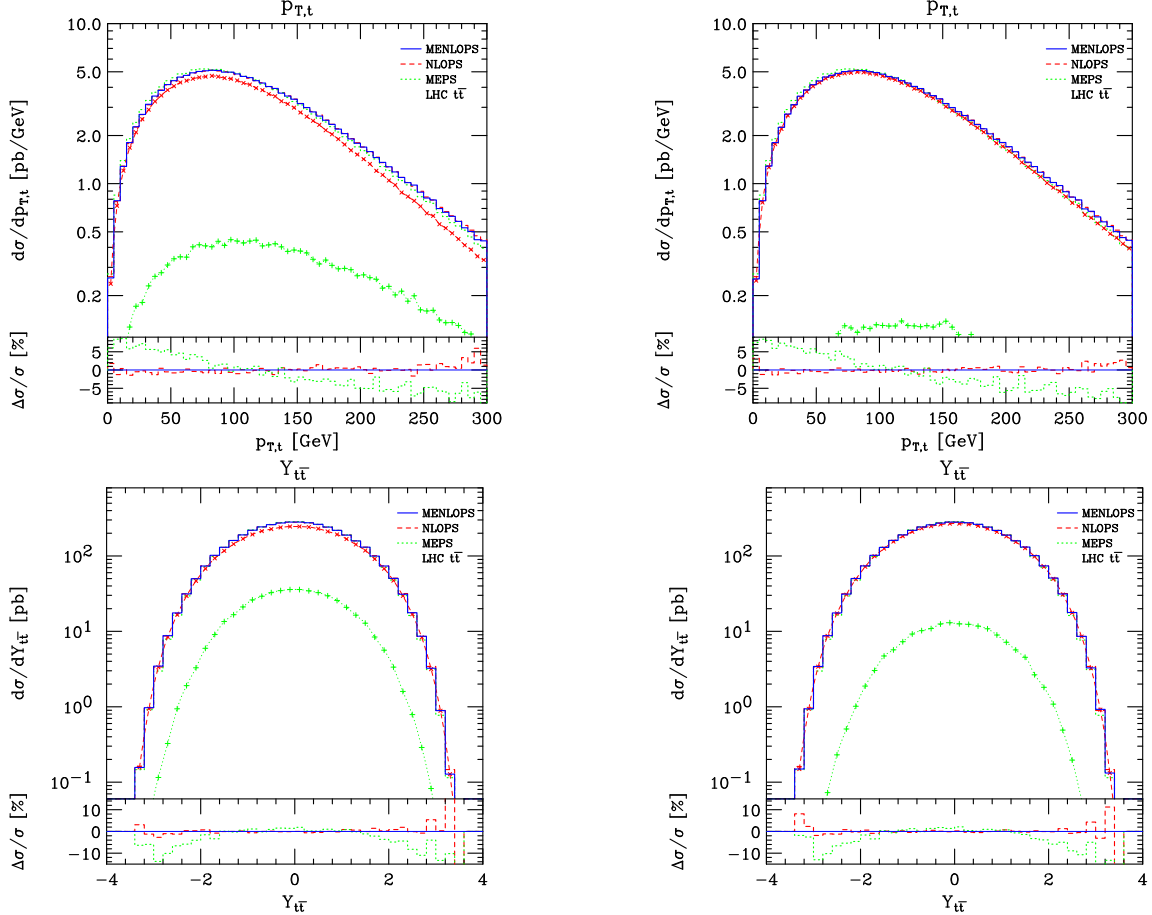


Figure 13: In the upper half of this figure we show the top quark transverse momentum in $t\bar{t}$ pair production using a 60 GeV (left) and 100 GeV (right) jet resolution scale in the MENLOPS merging procedure. The lower pair of plots shows, analogously, the rapidity distribution for the combined $t\bar{t}$ system. Despite the relatively large difference in the merging scales the combined MENLOPS prediction is stable with respect to the changing scale, showing deviations from the NLO result at the level of only 1 or 2% in both cases.

Appreciable differences of $\mathcal{O}(\alpha_S)$ can be seen in the shapes of the MEPS prediction of $Y_{t\bar{t}}$ with respect to those of the NLOPS/MENLOPS samples. We attribute this discrepancy to the absence of exact NLO corrections in the MEPS case. A similar trend was observed in the case of the W boson rapidity spectrum, for which the deviation in the shape was more prominent. Here, as in that case, we propose that these differences arise from a system-

atic bias of the MEPS approach, which produces the leading order final-state system more centrally than one expects on the grounds of pure LO and NLO computations (Sect. 4.3).

Figure 14 shows the transverse momentum distribution of the $t\bar{t}$ pair system. Here again the MENLOPS distribution is basically insensitive to the MEPS-NLOPS merging scale, always being within a few percent of the NLOPS prediction. It is clear, from the plot of the fractional differences, that the spectrum of the MEPS sample is around 20% lower than that of the NLOPS simulation. Note, however, that this difference is almost constant from around 50 GeV upwards, that is, the MEPS and NLOPS description of the *shape in that region* is in much better agreement than the 20% offset suggests. As noted above, the correspondence in the shapes of the distributions is important for the stability of the MENLOPS prediction there. The principal cause of the offset is in fact due to the 60% MEPS excess in the vicinity of the Sudakov peak which, on account of our rescaling the MEPS results so as to have the same weight as NLOPS events, makes the distribution of the former appear lower at larger p_T . This excess has actually already manifested itself in the form of an increased fraction of 0-jet events in the MEPS sample (Fig. 10).

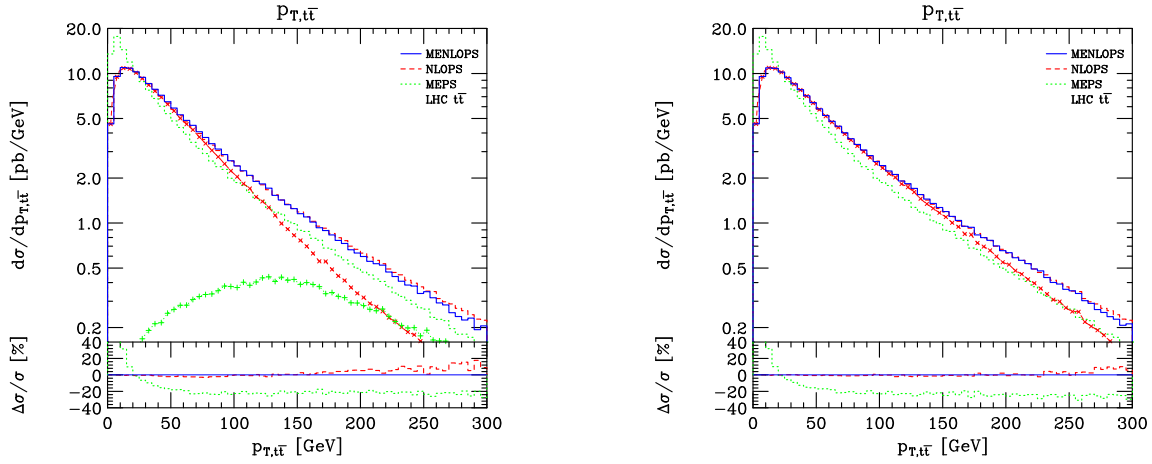


Figure 14: Above we show the transverse momentum distribution of the $t\bar{t}$ pair system using a 60 GeV (left) and 100 GeV (right) jet resolution scale as the MENLOPS merging scale. As in Figure 13, the greater resolution scale used in producing the MENLOPS sample (solid) on the right hand side, results in the MEPS component (dotted with + symbols) being greatly diminished. Nevertheless, the merged distribution very much assumes the form of the pure NLOPS prediction (dashed) to within $\mathcal{O}(1\%)$, with deviations only beginning to become noticeable in the high p_T tail, where contributions from events containing more than one jet become more important.

We have also reproduced this plot with the native PYTHIA $t\bar{t}$ simulation alone, without MEPS merging. Using the virtuality ordered shower, as for the MEPS sample, we find the same excess around the Sudakov peak. If, on the other hand, we use the transverse momentum ordered shower, we do not observe the excess, in fact we see nice agreement with POWHEG in the peak region. This is perhaps not surprising given that the generation of radiation in the POWHEG sample is wholly done according to evolution in p_T . Based on these observations we attribute the excess in the peak region to the different choices of

evolution variables. In particular, we note that the scale used to evaluate the PDF factors in the PYTHIA veto algorithm are the evolution variables themselves. However, just as p_T is the correct scale to use as the argument of the running coupling in the shower (the default in PYTHIA [26]), it is also the correct argument to use in evaluating the PDFs [5]. We therefore expect that the mismatch in scales leads to the sizeable differences in the soft region, at the parton level.

Having now taken this point into consideration, looking more closely at the plot of the fractional difference in Fig. 14, one can see that the shapes spectrum in the MEPS and MENLOPS are *still*, very slightly, softer than the pure NLOPS prediction at high p_T . To understand this, one should consider that the region of phase space in which the $t\bar{t}$ pair has a large transverse momentum is, naturally, to be associated with more energetic events and hence events with higher jet multiplicities. It follows from the MENLOPS algorithm, that in the limit that the $t\bar{t}$ pair transverse momentum tends to large values, the MEPS component of the MENLOPS sample will dominate. However we stress that, from the point of view of this observable, in this region of phase space, the higher order effects in the MEPS distribution in no way represent an improvement on the NLOPS prediction since the corresponding virtual corrections to $t\bar{t} + \text{jet}$ production are missing. Formally both approaches have the same degree of accuracy in describing the high p_T tail, with differences in the shapes being of higher order in α_S .

4.4.3 Jet activity

In Figure 15 we show the transverse momentum spectra of the hardest (left) and second hardest (right) jets, together with their corresponding rapidity distributions.

The distributions for the leading jet are predominantly given by that of the NLOPS simulation (dashed), with a structure reflecting the analogous $t\bar{t}$ pair distributions; moreover, the explanations for the structure are largely the same as in that case. The main difference between the leading jet transverse momentum and rapidity spectra, compared to those of the $t\bar{t}$ system, lies in the increased MEPS contribution to the MENLOPS predictions in the case of the leading jet. This is simply due to the fact that this is a less inclusive quantity. Whereas the $t\bar{t}$ pair distributions receive contributions from events with any number of jets (including no jets at all), those of the leading jet can only be constructed from events with at least one jet. Since the NLOPS contribution to the inclusive MENLOPS sample is made of 0- and 1-jet events only, it is then natural that one sees a substantial decrease in the fractional NLOPS component contributing to observables which exclude 0-jet events. Of, course, this does not represent any kind of problem since both MEPS and NLOPS simulations are only capable of describing such distributions with leading order, leading-log, accuracy.

By design, the MENLOPS algorithm completely excludes NLOPS events with two or more jets from the final sample, replacing them with MEPS events, since, for observables concerning the second jet, NLOPS predictions are not even accurate at leading order. The predictions for the second jet are therefore completely determined by the MEPS sample. This is easily seen to be the case by looking at the plots of the fractional differences, where one can see that the MENLOPS result is above the MEPS one by a constant factor (Eq. 3.6). As in the case of the leading jet, there is a tendency for the p_T spectra of the second hardest

jet to be softer in the MEPS/MENLOPS sample. This softening effect may run somewhat counter to the common lore surrounding shower Monte Carlo. However, it is well established that the parton shower approximation can lead to spectra harder than the true one.³ We also notice (see Figure 12) that for large jet multiplicities the NLOPS result is higher than the MEPS result, even if the latter is multiplied by an appropriate K -factor. We conclude that in $t\bar{t}$ production the MEPS method leads to slightly softer jets and slightly reduced activity in the event.

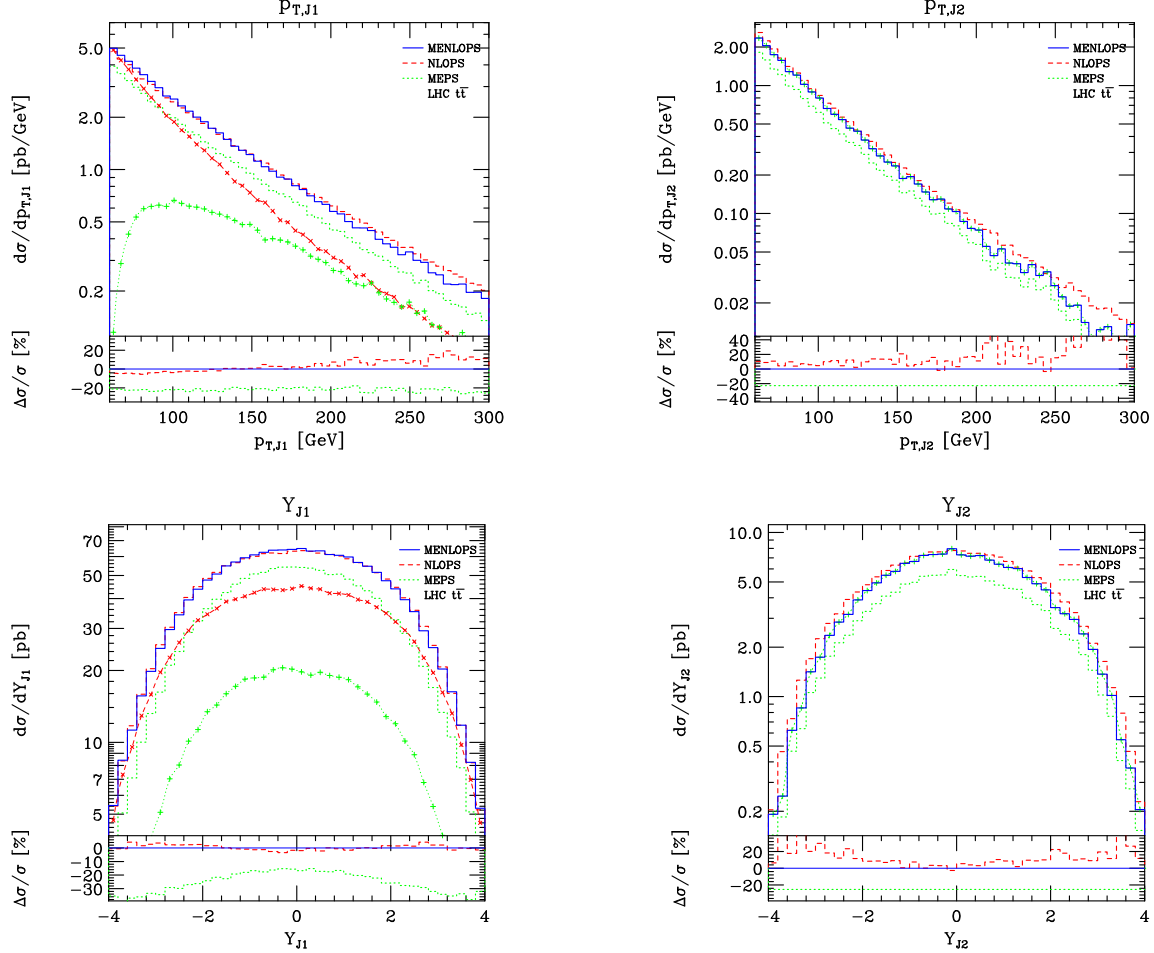


Figure 15: In the upper half of this figure we show the transverse momentum distribution of the hardest (left) and second hardest (right) jets, with the corresponding rapidity distributions shown underneath. The MENLOPS predictions (solid) shown here and their NLOPS (dashed) and MEPS (dotted) components were obtained from a MEPS-NLOPS combination with a merging scale of 60 GeV.

In the jet rapidity distributions we see a few puzzling features that may even seem to contradict some previous conclusions. Intuitively one expects, from simplified kinematical

³In fact, the ability of the shower to overestimate the rate of hard emissions is fundamental to *Matrix Element Correction* procedures, the forerunners of MEPS merging schemes, used to correct the pattern of radiation in the shower [26, 35, 36].

reasoning, that harder radiation and higher multiplicities should be associated with more activity in the central rapidity region. Since, in the present case, the NLOPS prediction exhibits the first two of these traits, albeit slightly, naively one may assume that the corresponding jet rapidity distributions should be more central than in the MEPS sample. However, in Figure 15 (by looking at the insert with the relative difference) we see the opposite behavior. We wish to quickly point out that the relative sizes of the differences in the p_T spectra should be borne in mind when considering these points. In the case of W production the second jet p_T spectrum was found to be approximately *five* times harder in the MEPS case with respect to the NLOPS one, and so the factor of two excess seen in the corresponding rapidity spectrum follows from simple kinematics considerations alone. On the contrary, here the differences are much smaller: the jet p_T spectra agree to within 30% in terms of their shape, as do their rapidity distributions. The same basic kinematic arguments are therefore not, by themselves, applicable in explaining the relationship between the jet p_T and rapidity distributions and the trends therein.

Whereas, in the case of the leading jet, the MENLOPS prediction is predominantly shaped by the NLOPS distribution, for the second jet it takes its form exclusively from the MEPS one. In both cases the NLOPS distributions are proportionally larger at larger rapidities with respect to the MEPS ones. We thus infer that some dynamical mechanism widens the rapidity spectrum in the NLOPS sample. One plausible mechanism must have to do with the virtual corrections implemented in the NLOPS simulation. In fact, in POWHEG a \bar{B}/B factor is present in the generation of *all* events, which depends upon the rapidity of the $t\bar{t}$ system; this may slightly suppress the central region with respect to the MEPS case. This hypothesis is substantiated by the known fact that NLO inclusive quantities in heavy flavour production display a remarkable proportionality to the corresponding LO ones, provided the same PDF sets are used⁴. Since NLO results include real emissions, and those should make the rapidity distributions more central, we must conclude that virtual corrections counteract this effect, and widen the rapidity spectrum. This line of argument is essentially the same as that taken earlier, in explaining the similar broadening effects seen in the case of the W boson and $t\bar{t}$ rapidity distributions. Put differently, in simpler terms: since the rapidity distribution of the $t\bar{t}$ system itself is broader in the NLOPS case, due to the inclusion of virtual corrections, given that the rapidity of the jets are strongly correlated with it (as can be seen in *e.g.* Fig. 16), it is natural to expect that they too have broader distributions.

The rapidity correlation between the second jet and the $t\bar{t}$ pair, shown in Fig. 16, echoes the tendency for the second jet to be more central in Fig. 15. Also this result may be related to the fact that large rapidities of the $t\bar{t}$ pair may be enhanced by virtual corrections, and that large differences between the second jet and the $t\bar{t}$ system rapidity may require a relatively large $t\bar{t}$ rapidity.

⁴We have explicitly confirmed this using independent code, in which we found the rapidity distribution of the top-quark pair at LO and NLO agreed to within $\pm 3\%$ in the region $|Y_{t\bar{t}}| < 3$, once the LO result was rescaled.

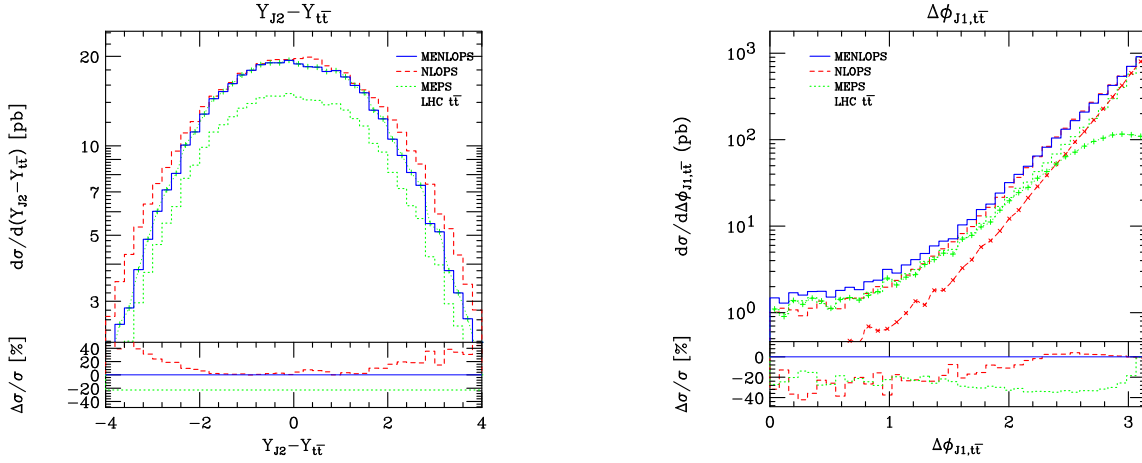


Figure 16: On the left we show the rapidity of the second hardest jet with respect to the $t\bar{t}$ pair, and on the right is the difference in azimuth between the leading jet and the $t\bar{t}$ system. Both of these distributions directly probe the jet structure in the events beyond that of the leading jet.

Figure 16 also shows the difference in azimuth between the leading jet and the $t\bar{t}$ system. Also this figure seems to suggest, that the radiation that accompanies the first jet is more collinear in the NLOPS sample than in the MEPS sample. In order to understand the plot, one should also keep in mind that the MEPS has a smaller fraction of single jet events than the NLOPS, due to the shape of the $t\bar{t}$ p_T spectrum displayed in Fig. 14. Also, from Fig. 10, we see that, for $y < 60$ GeV, the MEPS has a depleted single jet event multiplicity and an enhanced 0-jet fraction.

As with the distributions of the rapidity of the second jet and its rapidity correlation with respect to the $t\bar{t}$ system, this observable allows us to further probe the direction in which additional radiation is emitted. Recall that, in the NLOPS approach, the distribution of any jets in the event beyond the leading one originate from a parton shower description. Thus we expect the NLOPS sample to underpopulate the small $\Delta\Phi_{J1,t\bar{t}}$ region, an effect that was also seen in the corresponding W production distribution. In the MEPS case additional initial state radiation will tend to be more correlated with the direction of the incoming partons, while final state radiation will instead be correlated in angle with that of the leading jet (the progenitors), hence one expects, and indeed finds, proportionally more NLOPS events for which the jet and $t\bar{t}$ pair are back-to-back in azimuth than in the MEPS/MENLOPS samples.

We now end our analysis of top quark pair production by discussing the differential jet rates displayed in Figure 17. We remind the reader that the quantity, y_{nm} , being plotted in each histogram is the value of the clustering scale $\sqrt{d_{nm}}$, at which an n jet event becomes resolved as an $m = n + 1$ jet event. These distributions then probe directly the behavior of the MEPS and MENLOPS samples either side of their respective merging scale boundaries. Recall that the merging scale in the former sample was taken to be 30 GeV, while in the default MENLOPS combination a value of 60 GeV was taken. In both cases, different types of simulation populate either side of these unphysical boundaries, and so discontinuities could be expected to appear in these jet rates.

In the MEPS case the merging between the parton shower and the matrix elements involves a phase space partition for every different multiplicity. In the MENLOPS case all events with 0 or 1 jet are described by the one NLOPS simulation, with the MEPS sample alone describing the rest. Hence, in the latter case all jet rates should be free of discontinuities, with the exception, possibly, of the y_{12} jet rate, where there is an abrupt transition at 60 GeV from the MEPS description to the NLOPS one.

In all cases one can see that the predictions from the pure MEPS sample (dots) are smooth with no evidence of any merging scale dependence. Likewise the pure NLOPS results are also smooth, which has to be the case, given that the pure NLOPS sample involves no phase space partitions. The two distributions exhibit some differences in the soft region, the MEPS sample favoring more soft emission. This behavior was already noted in the discussion of the $t\bar{t}$ pair transverse momentum spectrum (Fig. 14), where an explanation based on the scales used to evaluate the PDFs was given.

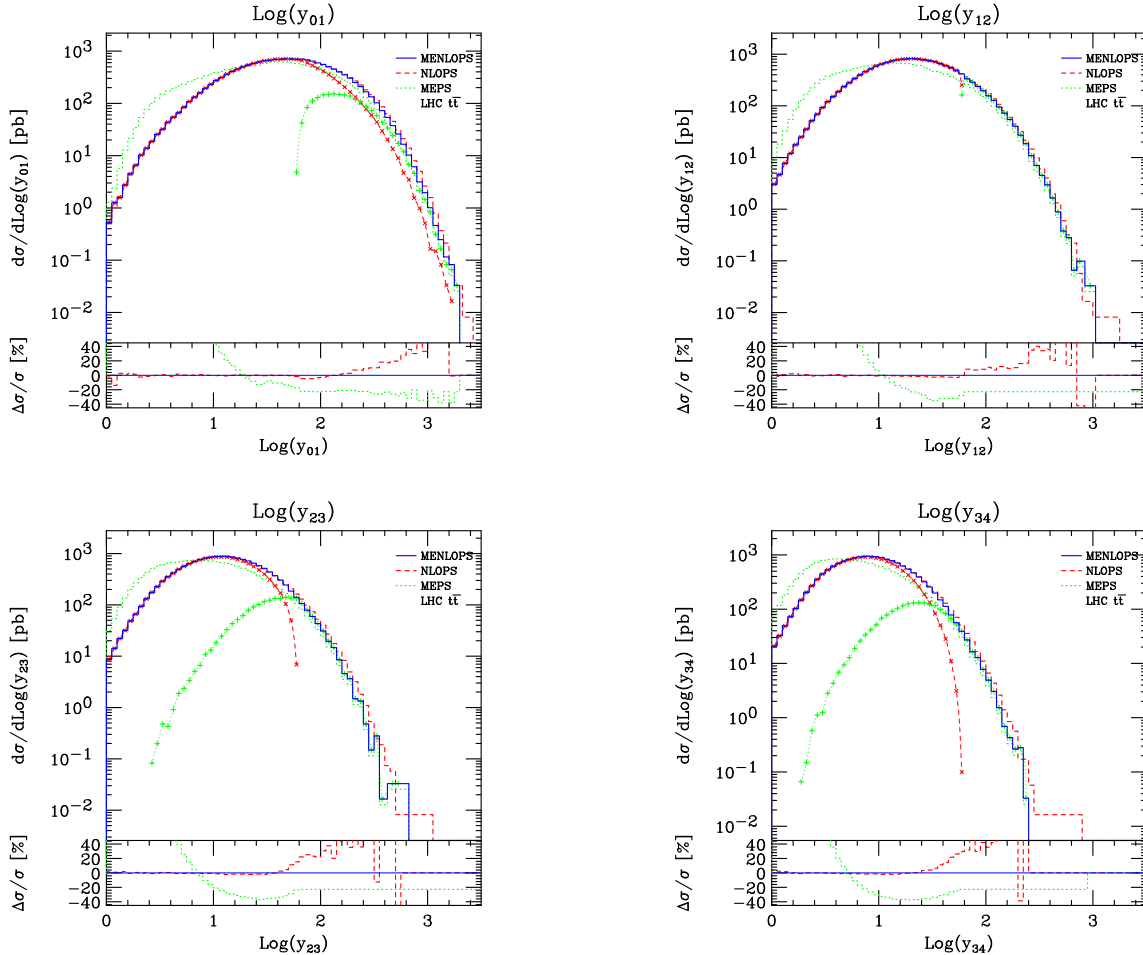


Figure 17: Here we show the logarithm of the value of the jet clustering scale y_{nm} at which an n -jet event is resolved as an $m = n + 1$ -jet event in each of the samples.

We also see that the MENLOPS predictions (solid) are similarly very smooth in all cases, in spite of the sharp transition from the NLOPS to the MEPS description in the y_{12}

distribution (their contributions to the MENLOPS sample are also shown). The reason for this smooth transition is simply due to the fact that the distributions constructed out of each class of events differ by sub-dominant terms but are, theoretically, the same at the level of large singular terms that are dominant around the 60 GeV threshold.

5. Conclusions

At the beginning of this document we have reviewed the next-to-leading order parton shower matching method POWHEG and re-examined matrix element-parton shower merging in the context of that formalism. Our initial aim has been to determine an exact means by which NLOPS simulations, in particular, POWHEG, may be combined with those implementing MEPS merging prescriptions, such as MLM and CKKW, so as to retain full NLO accuracy for inclusive observables and, at the same time, give an accurate description of multi-jet final states.

In Section 2, making use of rather modest assumptions concerning the behavior of an MEPS, we proposed a general expression for the corresponding hardest emission cross section which, in the POWHEG case, is key to achieving NLO accuracy. We have been able to reformulate these expressions in such a way as to identify how the MEPS simulation must be augmented, in order to make its hardest emission cross section converge with that of POWHEG. A key consideration in these manipulations has been the enforcement of unitarity in the MEPS approach, for all possible configurations of the underlying Born event. The conclusion of the theoretical analysis in Section 2 was that NLO accuracy and an accurate model of multi-jet radiation may be unified in a single simulation, by reweighting the MEPS events with a factor $\overline{B}(\Phi_B)/\overline{B}_{\text{ME}}(\Phi_B)$: the ratio of the NLO cross section, differential in the kinematics of the underlying Born event, divided by the MEPS simulation's leading order approximation to it. Note that the latter is not identical to the leading order cross section but exhibits differences at $\mathcal{O}(\alpha_S)$.

Despite the apparent simplicity of this conclusion, in general it is technically very challenging, since the multi-dimensional weight factors must be computed and stored prior to generating MEPS events (both of which are highly intensive numerical operations), which must then be followed by a further reweighting/rejection procedure. For simple processes, involving the production of just a single particle, the effort needed to realize the method is likely to be reasonable, as is the reduction in event generation efficiency. We leave this as the subject of a future study.

Motivated by the observation that MEPS merging schemes require, in practice, the introduction of a phase space partition for each jet multiplicity, beneath which radiation is described by the parton shower approximation, we were led to consider the question of to what extent it may be possible to achieve the same enhancements, by simpler means, without modifications to the *large, mature, existing*, body of simulations. It is clear that for events containing no additional jets, defined according to the MEPS merging scale, the NLOPS description is, categorically, always better than the MEPS one, while, for events with one additional jet the NLOPS is always at least as good (Sect. 3). With this in mind the preceding question becomes equivalent to the question: do events with two or more

jets, defined at the merging scale, comprise more than a fraction α_S of an inclusive MEPS merged sample?

Based on this we formulated a method for combining MEPS and NLOPS events into MENLOPS samples according to a further eponymous clustering scale. In this approach, if the MENLOPS merging scale can be set equal to the MEPS merging scale, without including more than a fraction $\mathcal{O}(\alpha_S)$ of the leading order, MEPS events, the resulting event sample is NLO accurate and the description of multi-jet final states is exactly as in the MEPS simulation. Requiring that the MEPS content not exceed a fraction $\mathcal{O}(\alpha_S)$ means that it may not always be possible to lower the MENLOPS merging scale to that used in a given MEPS sample. Since we always intend that the MENLOPS merging scale be restricted such that the fraction of, technically leading order, MEPS events in the sample is less than $\mathcal{O}(\alpha_S)$, to avoid compromising NLO accuracy, this approach should be viewed as a means of improving NLOPS simulations in the direction of MEPS ones, as opposed to the opposite sense.

In Section 4 we carried out a detailed analysis of MENLOPS samples for W^- and $t\bar{t}$ production. In the case of $t\bar{t}$ production we analyzed a sample merging MEPS and NLOPS events at a k_\perp clustering scale of 60 GeV, comprised of 12.5% MEPS events, 30 GeV above the merging scale recommended (and used) to create the MEPS sample with the PYTHIA virtuality ordered parton shower⁵. For W^- production the MENLOPS sample under study consisted of 96% NLOPS events, with the MEPS and NLOPS samples being merged at 25 GeV, only 5 GeV above that recommended for the MEPS sample. In view of this fact the implementation of the exact method for MEPS-NLOPS merging becomes an academic exercise in the case of W production. However, also in the $t\bar{t}$ case the practical gain from doing so is likely to be negligible.

In all cases, for inclusive quantities, the differences between the pure NLOPS and MENLOPS results were found to be negligible $\mathcal{O}(1\%)$. On the other hand differences of $\mathcal{O}(\alpha_S)$ can be seen in, for example, the W^- and $t\bar{t}$ rapidity distributions, when comparing the NLOPS and MENLOPS predictions to those from the MEPS simulation. We attribute these to the absence of NLO corrections in the latter. Semi-inclusive observables, probing the distribution of the leading jet, exhibit differences between the pure NLOPS and MEPS results, with the MENLOPS prediction, naturally, lying between the two. These $\mathcal{O}(\alpha_S)$ differences are, however, expected, since all techniques here have only LO accuracy for such quantities. By contrast, for observables directly sensitive to the second hardest jet, the MEPS and MENLOPS results become identical and reveal large corrections when compared to those of the NLOPS method. These corrections are particularly acute in the case of W^- production.

In conclusion we wish to recommend the MENLOPS procedure as a transparent and versatile means to pool existing Monte Carlo resources together, in a way which encapsulates to a large extent all of their best qualities.

⁵We remind the reader that the recommended MEPS merging scale in the case of the transverse momentum ordered shower was 100 GeV [16].

6. Acknowledgments

Keith Hamilton would like to thank Simon de Visscher and Rikkert Frederix for encouraging us to use MADGRAPH, with which our experience was all very positive. We are also very grateful to the CP3, Louvain-la-Neuve, especially Pavel Demin and Fabio Maltoni, for access to the excellent computing facilities there.

References

- [1] S. Frixione and B. R. Webber, *Matching NLO QCD Computations and Parton Shower Simulations*, *JHEP* **06** (2002) 029, [[hep-ph/0204244](#)].
- [2] P. Nason, *A new method for combining NLO QCD with shower Monte Carlo algorithms*, *JHEP* **11** (2004) 040, [[hep-ph/0409146](#)].
- [3] S. Frixione, P. Nason, and C. Oleari, *Matching NLO QCD computations with Parton Shower simulations: the POWHEG method*, *JHEP* **11** (2007) 070, [[arXiv:0709.2092](#)].
- [4] S. Frixione, P. Nason, and B. R. Webber, *Matching NLO QCD and parton showers in heavy flavour production*, *JHEP* **08** (2003) 007, [[hep-ph/0305252](#)].
- [5] P. Nason and G. Ridolfi, *A positive-weight next-to-leading-order Monte Carlo for Z pair hadroproduction*, *JHEP* **08** (2006) 077, [[hep-ph/0606275](#)].
- [6] S. Frixione, P. Nason, and G. Ridolfi, *A Positive-Weight Next-to-Leading-Order Monte Carlo for Heavy Flavour Hadroproduction*, *JHEP* **09** (2007) 126, [[arXiv:0707.3088](#)].
- [7] S. Alioli, P. Nason, C. Oleari, and E. Re, *NLO vector-boson production matched with shower in POWHEG*, *JHEP* **07** (2008) 060, [[arXiv:0805.4802](#)].
- [8] K. Hamilton, P. Richardson, and J. Tully, *A Positive-Weight Next-to-Leading Order Monte Carlo Simulation of Drell-Yan Vector Boson Production*, *JHEP* **10** (2008) 015, [[arXiv:0806.0290](#)].
- [9] S. Alioli, P. Nason, C. Oleari, and E. Re, *NLO Higgs boson production via gluon fusion matched with shower in POWHEG*, *JHEP* **04** (2009) 002, [[arXiv:0812.0578](#)].
- [10] K. Hamilton, P. Richardson, and J. Tully, *A Positive-Weight Next-to-Leading Order Monte Carlo Simulation for Higgs Boson Production*, *JHEP* **04** (2009) 116, [[arXiv:0903.4345](#)].
- [11] S. Frixione, E. Laenen, P. Motylinski, B. R. Webber, and C. D. White, *Single-top hadroproduction in association with a W boson*, *JHEP* **07** (2008) 029, [[arXiv:0805.3067](#)].
- [12] S. Alioli, P. Nason, C. Oleari, and E. Re, *NLO single-top production matched with shower in POWHEG: s- and t-channel contributions*, *JHEP* **09** (2009) 111, [[arXiv:0907.4076](#)].
- [13] P. Nason and C. Oleari, *NLO Higgs boson production via vector-boson fusion matched with shower in POWHEG*, *JHEP* **02** (2010) 037, [[arXiv:0911.5299](#)].
- [14] P. Torrielli and S. Frixione, *Matching NLO QCD computations with PYTHIA using MC@NLO*, [arXiv:1002.4293](#).
- [15] M. L. Mangano, M. Moretti, F. Piccinini, and M. Treccani, *Matching matrix elements and shower evolution for top- quark production in hadronic collisions*, *JHEP* **01** (2007) 013, [[hep-ph/0611129](#)].

- [16] J. Alwall, S. de Visscher, and F. Maltoni, *QCD radiation in the production of heavy colored particles at the LHC*, *JHEP* **02** (2009) 017, [[arXiv:0810.5350](#)].
- [17] M. L. Mangano, M. Moretti, F. Piccinini, R. Pittau, and A. D. Polosa, *ALPGEN, a generator for hard multiparton processes in hadronic collisions*, *JHEP* **07** (2003) 001, [[hep-ph/0206293](#)].
- [18] J. Alwall *et. al.*, *MadGraph/MadEvent v4: The New Web Generation*, *JHEP* **09** (2007) 028, [[arXiv:0706.2334](#)].
- [19] T. Gleisberg *et. al.*, *Event generation with SHERPA 1.1*, *JHEP* **02** (2009) 007, [[arXiv:0811.4622](#)].
- [20] S. Alioli, P. Nason, C. Oleari, and E. Re, *A general framework for implementing NLO calculations in shower Monte Carlo programs: the POWHEG BOX*, [arXiv:1002.2581](#).
- [21] W. T. Giele, D. A. Kosower, and P. Z. Skands, *A Simple shower and matching algorithm*, *Phys. Rev.* **D78** (2008) 014026, [[arXiv:0707.3652](#)].
- [22] N. Lavesson and L. Lonnblad, *Extending CKKW-merging to One-Loop Matrix Elements*, *JHEP* **12** (2008) 070, [[arXiv:0811.2912](#)].
- [23] Z. Nagy and D. E. Soper, *Parton showers with quantum interference*, *JHEP* **09** (2007) 114, [[arXiv:0706.0017](#)].
- [24] S. D. Ellis and D. E. Soper, *Successive combination jet algorithm for hadron collisions*, *Phys. Rev.* **D48** (1993) 3160–3166, [[hep-ph/9305266](#)].
- [25] S. Catani, Y. L. Dokshitzer, M. H. Seymour, and B. R. Webber, *Longitudinally invariant K_t clustering algorithms for hadron hadron collisions*, *Nucl. Phys.* **B406** (1993) 187–224.
- [26] T. Sjostrand, S. Mrenna, and P. Z. Skands, *PYTHIA 6.4 Physics and Manual*, *JHEP* **05** (2006) 026, [[hep-ph/0603175](#)].
- [27] J. Alwall *et. al.*, *MadGraph / MadEvent Wiki*, <http://cp3wks05.fynu.ucl.ac.be/twiki/bin/view/Main/WebHome> (2007).
- [28] J. Alwall *et. al.*, *Comparative study of various algorithms for the merging of parton showers and matrix elements in hadronic collisions*, *Eur. Phys. J.* **C53** (2008) 473–500, [[arXiv:0706.2569](#)].
- [29] S. Frixione, P. Nason, and G. Ridolfi, *The POWHEG-hvq manual version 1.0*, [arXiv:0707.3081](#).
- [30] A. D. Martin, R. G. Roberts, W. J. Stirling, and R. S. Thorne, *Uncertainties of predictions from parton distributions. 1: Experimental errors*, *Eur. Phys. J.* **C28** (2003) 455–473, [[hep-ph/0211080](#)].
- [31] M. R. Whalley, D. Bourilkov, and R. C. Group, *The Les Houches Accord PDFs (LHAPDF) and Lhagluue*, [hep-ph/0508110](#).
- [32] M. Cacciari and G. P. Salam, *Dispelling the N^3 myth for the k_t jet-finder*, *Phys. Lett.* **B641** (2006) 57–61, [[hep-ph/0512210](#)].
- [33] Y. L. Dokshitzer, D. Diakonov, and S. I. Troian, *Hard Processes in Quantum Chromodynamics*, *Phys. Rept.* **58** (1980) 269–395.
- [34] F. Krauss, A. Schalick, S. Schumann, and G. Soff, *Simulating W/Z +jets production at the CERN LHC*, *Phys. Rev.* **D72** (2005) 054017, [[hep-ph/0503280](#)].

- [35] M. H. Seymour, *Matrix element corrections to parton shower algorithms*, *Comp. Phys. Commun.* **90** (1995) 95–101, [[hep-ph/9410414](#)].
- [36] M. H. Seymour, *A Simple prescription for first order corrections to quark scattering and annihilation processes*, *Nucl. Phys.* **B436** (1995) 443–460, [[hep-ph/9410244](#)].